sustainability

Article

Sustainable Design: Minimizing Discomfort Glare Through Data-Driven Methods for Responsive Facades

Negar Heidari Matin [1,*], Ali Eydgahi [2] and Amin Gharipour [3]

[1] Gibbs College of Architecture, University of Oklahoma, Norman, OK 73019, USA
[2] School of Engineering, Eastern Michigan University, Ypsilanti, MI 48197, USA; aeydgahi@emich.edu
[3] School of ICT, Griffith University, Brisbane, QLD 4111, Australia
* Correspondence: negar.matin@ou.edu

Abstract: Ensuring visual comfort for occupants in sustainable buildings involves addressing discomfort glare and its associated risks. Responsive facades, designed based on pre-set algorithms, enhance visual performance and reduce discomfort glare by continuously adapting to changes in daylight intensity, reflection, or color. In this study, computational models were developed by incorporating hourly daylight glare probability (DGP) with occupants' spatial data and facade active variables to minimize discomfort glare for responsive facades. To evaluate these models, a room with an office setting was parametrically simulated with a responsive facade, generating hourly DGP data for an entire year across different facade configurations, building orientations, and climate zones. The Exhaustive Search Algorithm was then used to calculate the optimal hourly angles for the facade configurations. The results indicate that the proposed models can significantly maintain DGPs within an imperceptible range (<0.35) in all scenarios compared to a no-louver scenario. These models offer valuable insights for architects, facade designers, and researchers aiming to enhance occupant visual comfort and productivity through innovative responsive facade strategies. Aligning visual comfort, well-being, and productivity with sustainability ensures that buildings operate efficiently while providing a healthy and comfortable environment for users.

Keywords: Responsive facades; facade optimization; visual comfort; glare; data-driven design

Academic Editors: Vincenzo Costanzo and Antonio Caggiano

Received: 22 September 2024
Revised: 29 December 2024
Accepted: 15 January 2025
Published: 20 January 2025

Citation: Matin, N.H.; Eydgahi, A.; Gharipour, A. Sustainable Design: Minimizing Discomfort Glare Through Data-Driven Methods for Responsive Facades. *Sustainability* **2025**, *17*, 783. https://doi.org/10.3390/su17020783

1. Introduction and Background

People spend a significant amount of time in offices [1]. The interior layout, lighting and visual comfort, temperature and thermal comfort, noise and acoustic comfort, biophilia, and outside window views of office settings can affect the physical and mental health of office workers [2]. Visual comfort is crucial, as it directly affects human photosensory perception and can influence office workers' abilities to perform various tasks [3]. Visual comfort relies on several factors, including light intensity, light uniformity, color rendering quality, and the potential for glare [4]. Among these factors, glare is widely acknowledged as the most significant factor for ensuring occupants' health, comfort, and task performance [5].

According to the International Commission on Illumination (CIE), glare is defined as a "condition of vision in which there is discomfort or a reduction in the ability to see details or objects, caused by an unsuitable distribution or range of luminance, or by extreme contrasts" [6]. Discomfort glare is further defined by the CIE as "glare that causes discomfort without necessarily impairing the vision of objects" [7]. Therefore, the term 'discomfort' is used to distinguish between a subjective sensation (discomfort from glare) and an impairment to visual performance (disability from glare)—in other words, between the psychological glare (discomfort) and physiological glare disability [8].

The conducted research has shown that glare can result in various eye and health issues, including cataracts, dry eyes, macular degeneration, retinal inflammation, fatigue, light sensitivity, migraines, headaches, and nervous system disturbances. These problems can range from mild eye discomfort to severe vision loss in office spaces [9,10]. Managing glare could improve cognitive performance and employees' satisfaction, concentration, and mood and reduce headaches and eyestrain [11–13].

While the literature considers two types of glare, disability glare and discomfort glare [14], glare-related metrics predominantly focus on discomfort glare [15]. Discomfort glare is a multifaceted phenomenon, which makes its assessment challenging [16].

The complexity of discomfort glare arises from both temporal and spatial variations. Discomfort glare depends on the user's position and viewing direction and is influenced by the dynamically changing luminance of the sky dome. Additionally, material properties and geometrical aspects (i.e., optical window properties, movable shading devices with specific geometry and materials, etc.) further complicate the evaluation of discomfort glare [17].

A number of different metrics were proposed to quantify the discomfort glare perceived by building occupants. Most of them were developed and validated for only glare conditions caused by artificial light sources [8,16,17]. However, among the proposed discomfort glare metrics, daylight glare probability (DGP) is widely used in the literature since it offers a stronger correlation with the occupants' responses in terms of glare sensation compared to other glare metrics [3].

The discomfort glare metrics, such as Unified Glare Rating (UGR), Discomfort Glare Index (DGI), CIE Glare Index (CGI), and Visual Comfort Probability (VCP), just focus on the contrast ratio between the background's average luminance and the glare source's luminance, whereas the DGP also includes an evaluation of the level of illuminance perceived by the occupant by means of the term vertical eye illuminance (Ev) [18]. Conversely, a limitation of incorporating DGP is that it typically involves a lot more computation time and user effort compared to the simple analytic calculations required by most of the other glare metrics [19]. Assessing DGP is a time-consuming task due to several factors. The complexity of glare prediction models, which take into account parameters such as window size and shading devices, necessitates thorough analysis and computation. Additionally, annual DGP analysis involves generating high-dynamic-range (HDR) images for each time-step (typically one hour) throughout the year, which is a resource-intensive process. Furthermore, interreflection calculations within the scene contribute to computation time. Lastly, occupant assessments for glare validation further increase the overall time investment [20].

For the DGP computation process, one or more viewpoints of interest in the eye level in a specific point of the room have been chosen to correspond to occupant positions to produce renderings in the Radiance with the HDR picture format. Finally, a glare evaluation has to be carried out using Evalglare, a Radiance-based tool developed to detect glare sources on a 180° fish-eye scene [21]. It needs to be mentioned that the DGP is dependent on the position and direction of view of the occupants, which means that the calculation should be repeated for all relevant points and directions in a space [16].

Reviewing the existing literature reveals that a reliable prediction of glare using metrics still poses significant challenges in the building since discomfort glare depends on the occupant's position, occupant's background, occupant's eyes capabilities to adapt to the light environment, occupant's tolerance to discomfort glare, range of assessed luminance, and vertical illuminance in the eyes' field [19]. While most of the discomfort glare causes are subjective to the occupants' age, gender, and behavior toward indoor conditions, it is still possible to measure, control, and optimize the occupant's position; the luminance of the glare source; the solid angle of the glare source; and the vertical illuminance in the eyes' field [22].

Building facades are the primary sources of daylight penetration, affecting the intensity, color, distribution of daylight, and discomfort glare in the interiors [19,22]. Compared to other types of facades, responsive facades could yield enhanced visual performance and reduced discomfort glare, mainly due to their ability to continuously adjust their functions, features, or behavior over time in response to environmental stimuli, as well as occupants' preferences and needs [23–26]. This continuous adjustment, which leads to the optimum performance of responsive facades, contributes to building sustainability by minimizing energy consumption and greenhouse gas emissions while promoting a more sustainable and eco-friendly approach to building design.

Enhanced visual performance with responsive facades is affected by two types of variables, active and passive, that are used in the design [27–29]. Passive design variables are considered to be fixed in response to external stimuli and internal factors, such as infiltration, window-to-wall ratio, glazing types, and wall insulation [30]. In contrast, active design variables can adapt to external stimuli and internal factors, such as the louvers' angles, the facade's porosity (area/depth), and the granularity of the facade [31]. The maximum performance of responsive facades can be guaranteed by choosing an efficient adaptive strategy for active design variables [32]. As an efficient adaptive strategy, time increments of active design variables can improve facade performance, minimizing discomfort glare and maximizing occupant visual comfort when matched with hourly changes in daylight patterns [30].

Among studies on the performance of responsive facades [23,33–42], no studies elaborate on minimizing the cost function of discomfort glare with multiple design scenarios, and most research has been focused on the design of responsive facades, prioritizing architectural form studies/analyses while evaluating the performance of facades with inadequate illuminance and glare simulations [23,33–42]. Also, limited studies have investigated discomfort glare and its related metrics compared to those focusing on illuminance and its associated metrics [26,43]. Due to the high computation time of glare simulation, these studies have typically evaluated discomfort glare in only one point/location as an occupant position/location in a room with a single view direction, without considering various possible design factors such as time increments, occupant's locations, occupant's sight directions, facade orientations, and building locations/climate zones [44–46]. Consequently, their glare calculations cannot provide realistic glare evaluations due to a lack of sufficient design factors.

Focusing on design variables such as active angles of louvers, this research proposes a computer model aimed at minimizing DGPs in a simulated commercial office room with responsive facades, considering occupants' positions, occupants' view directions, and hourly active angles of louvers as dependent variables. A set of computer-aided design software is utilized to calculate, evaluate, and analyze DGPs for a year in the simulated office room, while hourly adaptation angles are rotated for hourly daylight patterns. The proposed model investigates the possibility of discomfort glare in all possible occupants' positions with multiple view directions. Then, a computational algorithm is utilized to identify the optimum hourly angles based on average discomfort glare observed for both horizontal and vertical facade configurations in four different facade orientations (N, E, S, W) and four different facade locations/climates. Aligning visual comfort, well-being, and productivity with sustainability ensures that the building operates efficiently while providing a healthy and comfortable environment for its users.

2. Methodology Used

Being the most reliable glare metric, DGP is widely used as a short-term, local, one-tailed metric, which is developed from empirical research with human subjects [47,48]. Assuming that the vertical eye illuminance produced by the light source [lux] is represented by E_V; the luminance of the source [cd/m^2] is denoted by L_s; the solid angle of the source seen by an occupant is represented by Ks; and the position index is indicated by P, the DGP can be calculated as follows:

$$DGP = 5.87 \cdot 10^{-5} E_V + 0.0918 \cdot log\left[1 + \sum_{i=1}^{n}\left(\frac{L_{si}^2 \times K_{si}}{E_v^{1.87} \cdot P_i^2}\right)\right] \quad (1)$$

It is notable that the position index uses the occupant's line of sight to measure the experienced discomfort glare relative to the angular displacement of the source (azimuth and elevation) from [49–51].

Equation (1) is applicable for daylight glare probability (DGP) values that fall within the range of 0.2 to 0.8 and is also valid for situations where the vertical eye illuminance is greater than 380 lux. The ranges of glare sensations can be categorized as imperceptible when the DGP is less than 0.35, perceptible when the DGP is between 0.35 and 0.4, disturbing when the DGP is between 0.4 and 0.45, and intolerable when the DGP exceeds 0.45 [48].

Focusing on a specific point x in the office room, the DGP can be optimized using the following objective function:

$$obj_x = \int_{\theta_{View}} w_{\theta_{View}} F(Active\ variables,\ Passive\ variables) d\theta_{View} \quad (2)$$

where θ_{Viwe} is the view angle, $w_{\theta_{Viwe}}$ denotes the weight assigned to each θ_{Viwe}, and F presents the obtained DGP value based on active and passive variables.

This study utilized the louver angle as an active design variable, which can be adjusted hourly to accommodate varying hourly daylight patterns. Consequently, Equation (2) can be re-formulated as follows:

$$obj_{x,\ \theta} = \int_{\theta_{View}} w_{\theta_{View}} F(\theta) d\theta_{View} \quad (3)$$

where θ is the angle of the louver movement. By incorporating $h \in H$, representing the hours of the day, and N, showing the total number of possible pairs of occupants' positions and angles of view directions, Equation (3) can be formulated as follows:

$$obj_{x,\ \theta,\ h} = \frac{1}{N} \int_H \int_{\theta_{View}} w_{\theta_{View}} F(\theta) d\theta_{View} dh \quad (4)$$

Finally, the optimization problem using the obj$x$, θ, h can be developed as follows:

$$Minimize\ obj_{x,\ \theta,\ h}\ subject\ to\ \theta \in \Theta \quad (5)$$

The outcomes of Equation (5) can be found by exploring the set of available angles $\theta \in \Theta$ and identifying the optimal value of θ for each $h \in H$.

3. Evaluation of Various Design Scenarios

Rhinoceros version 6.0 software was employed to create a standard office space measuring 4.0 m in width, 9.0 m in depth, and 3.0 m in height, as shown in Figure 1a. The thicknesses of the walls, ceiling, and flooring elements were designed to be 0.15 m, 0.12 m, and 0.12 m, respectively. An opening was simulated for the office room with dimensions of 2.6 m as width and 3.6 m as length. The simulated window was made from Azuria-Sungate

400 (3) with a Solar Heat Gain Coefficient (SHGC) of 0.332 and a Visible Light Transmission (TVIS) of 0.58 that was installed on the smaller side of the office room. Natural light was considered the only source of light in the office room, with no artificial lighting inside. Grasshopper, a visual programming and simulation tool compatible with Rhinoceros 3D, was employed to parametrically simulate a responsive facade system and to apply it to the office window. Then, to investigate various design scenarios, the simulated office room could be oriented toward the four primary main directions (north, west, south, and east). A range of 180 degrees, starting from −90 degrees, segmented into 60 steps with increments of 3 degrees is used for horizontal and vertical louver angle rotations in a clockwise direction, as shown in Figure 1a.

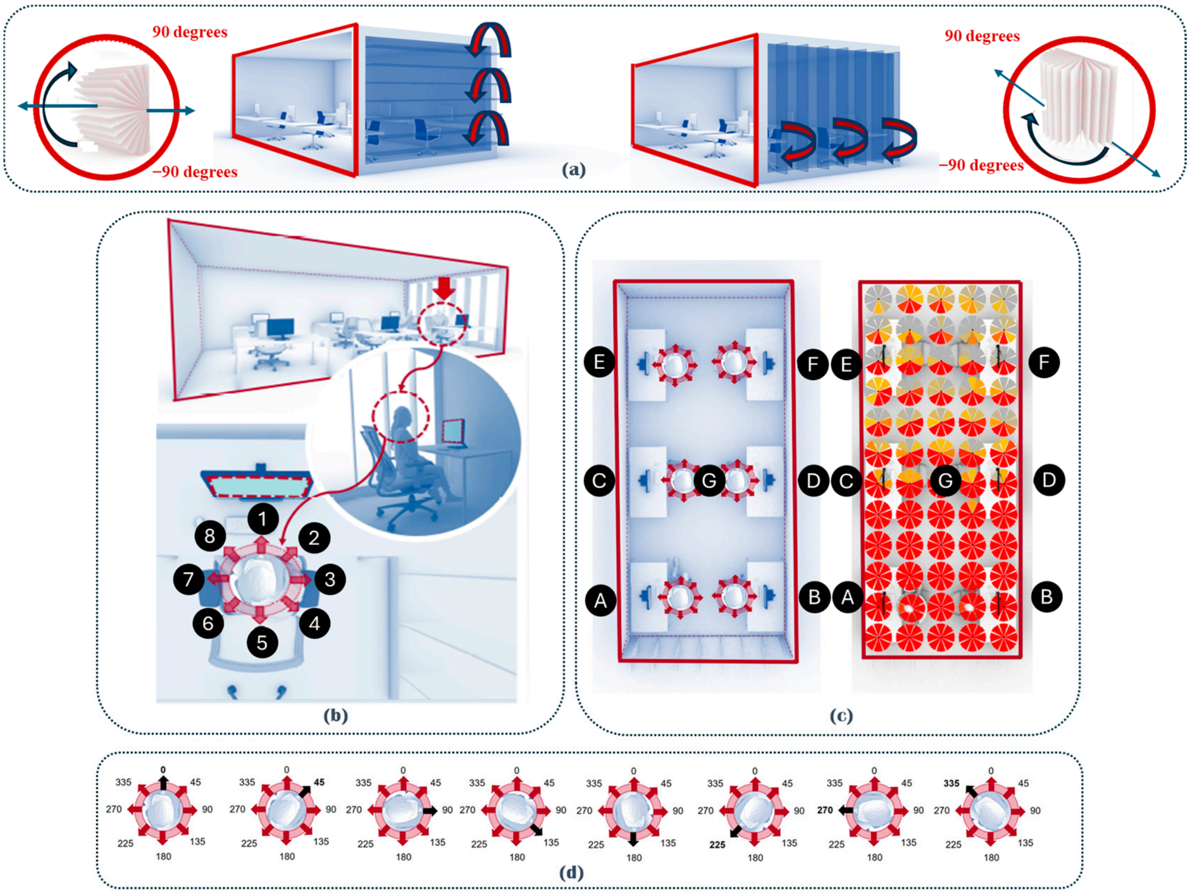

Figure 1. (**a**) Simulated office room with horizontal and vertical responsive louvers; (**b**) occupants' position; (**c**) 60 sensors distribution across the office; (**d**) various view angles of occupants. The labels A through G show the workspaces have been labeled as A through F letters. Also, the center point of the office room is named point G. The numbers 1 through 8 present various eight angles with 45-degree intervals for moving occupants corneal plane.

The simulated responsive facades feature seven horizontal and seven vertical louvers, each measuring 3 m by 0.26 m by 0.18 m, with spacing set at 0.4 m for the horizontal and 0.5 m for the vertical configurations. These louvers, which were simulated from dark gray aluminum, have a reflectance of 19.36%, a specular component of 1.65%, a diffuse component of 17.70%, and a roughness of 0.2, utilizing Rhinoceros's plug-in for daylight and energy simulations, which is named Climate Studio and has been validated by other researchers through validation of Radiance as its core engine [52,53]. The annual daylight glare probability was assessed using a grid-based approach, with 60 sensors positioned on a horizontal grid plane at a height of 1.2 m above the office floor. This height corresponds to the standard corneal plane level for occupants seated and performing typical office tasks, as shown in Figure 1b,c. The sensors were positioned approximately 0.8 m apart in both directions on the plane to simulate the potential seating positions of occupants throughout the office space. It was assumed that occupants with normal vision could rotate their corneal plane by moving their necks from 0 to 360 degrees, allowing for a range of viewing angles and orientations as illustrated in Figure 1c. Then, vertical illuminance with the eye height received by occupants was measured in various eight angles with 45-degree intervals, while occupants' positions were changed/manipulated to 60 points across the office room, as shown in Figure 1d.

Three assumptions are made about the office room and its occupants. The first one is that the office room will be occupied for ten hours, from 8:00 a.m. to 6:00 p.m. This schedule agrees with the IESNA's new Lighting Measurement IES LM-83-12 [43,54]. The second assumption is that six workspaces are occupied by office workers performing regular office work, as shown in Figure 1b. The workspaces have been labeled as A through F letters. Also, the center point of the office room is named point G. The third assumption is that the office workers in the assumed office space demonstrate efficient and effective visual performance, especially in situations involving discomfort glare. They possess healthy visual abilities, including visual acuity, proper eye coordination, depth perception, color vision, and the ability to focus and maintain clear vision for extended periods without experiencing eye strain or fatigue [55].

The following design scenarios were utilized in this study:

1. Fixed horizontal and vertical louvers with an angle of zero degrees.
2. The angles of the louvers were fixed at 0 degrees. They were not able to rotate horizontally or vertically in response to daylight patterns during the day.
3. Responsive horizontal and vertical louvers with hourly optimum angles using the proposed computation model.
4. The angles of louvers were capable of hourly rotation horizontally or vertically from −90 degrees to +90 degrees in response to daylight patterns during the day.

The design scenarios of fixed louvers were compared with two configurations of optimum responsive louvers. These scenarios were repeated parametrically for four facade orientations (N, W, S, E) and different facade locations/climate zones.

Among all cities categorized by ASHRAE climate classification, four cities from different climate zones in the United States, namely Miami (FL), Phoenix (AZ), Boston (MA), and Milwaukee (WI) were selected using K-cluster analysis along with an elbow method [56,57]. The sky condition for the DGP simulation was assumed to be set in the clear sky with the sun. Typical annual meteorological data provided as an EnergyPlus Weather File (EPW) by the U.S. Department of Energy were utilized for the selected cities/climate zones. Annual meteorological data of the selected cities were adopted to simulate the hourly indoor vertical illuminance associated with the different scenarios. Based on the ASHRAE classification, Miami and Phoenix represent the very Hot–Humid (1A) and Hot–Dry (2B) climates, respectively. Boston and Milwaukee represent Cool–Humid (5A) and Cold–Humid (6A) climates, respectively [58].

4. Results and Discussions

The following settings were applied for daylight glare probability estimation: Hourly indoor vertical illuminances were calculated at sixty predefined sensors with eight different view angles during every 8760 h of a year, while the responsive louver angles were parametrically changed from −90 degrees to +90 degrees. Eight view angles were defined, and the $w_{\theta_{View}}$ was set to [1,1,1,1,1,1,1,1]. The measurements were repeated for four facade orientations, two horizontal and vertical façade configurations, and four cities/climate zones. The simulations ran 20,736,200 times, and daylight glare probability values at

995,328,000 points were calculated and stored. Postgres-SQL was integrated with R to handle the simulation data management and deploy the optimization process using brute-force search. A brute-force search algorithm is a method that exhaustively explores all possible solutions to an optimization problem. It systematically evaluates each candidate solution, starting from the first possibility and proceeding sequentially through all options. However, it can computationally be expensive due to the need to consider all possibilities [59]. The selection of an efficient algorithm largely depends upon the specific conditions of the simulation experiment. Although more efficient algorithms may exist for certain scenarios, the brute-force algorithm emerged as the optimal choice for this study due to the substantial volume of data [60]. Figure 2 shows the flow and execution of the data in the simulation. There are alternative optimization techniques that could potentially offer improved computational efficiency. For example, heuristic techniques, such as simulated annealing, genetic algorithms, and particle swarm optimization, can be applied to solve the proposed optimization problem [61–64].

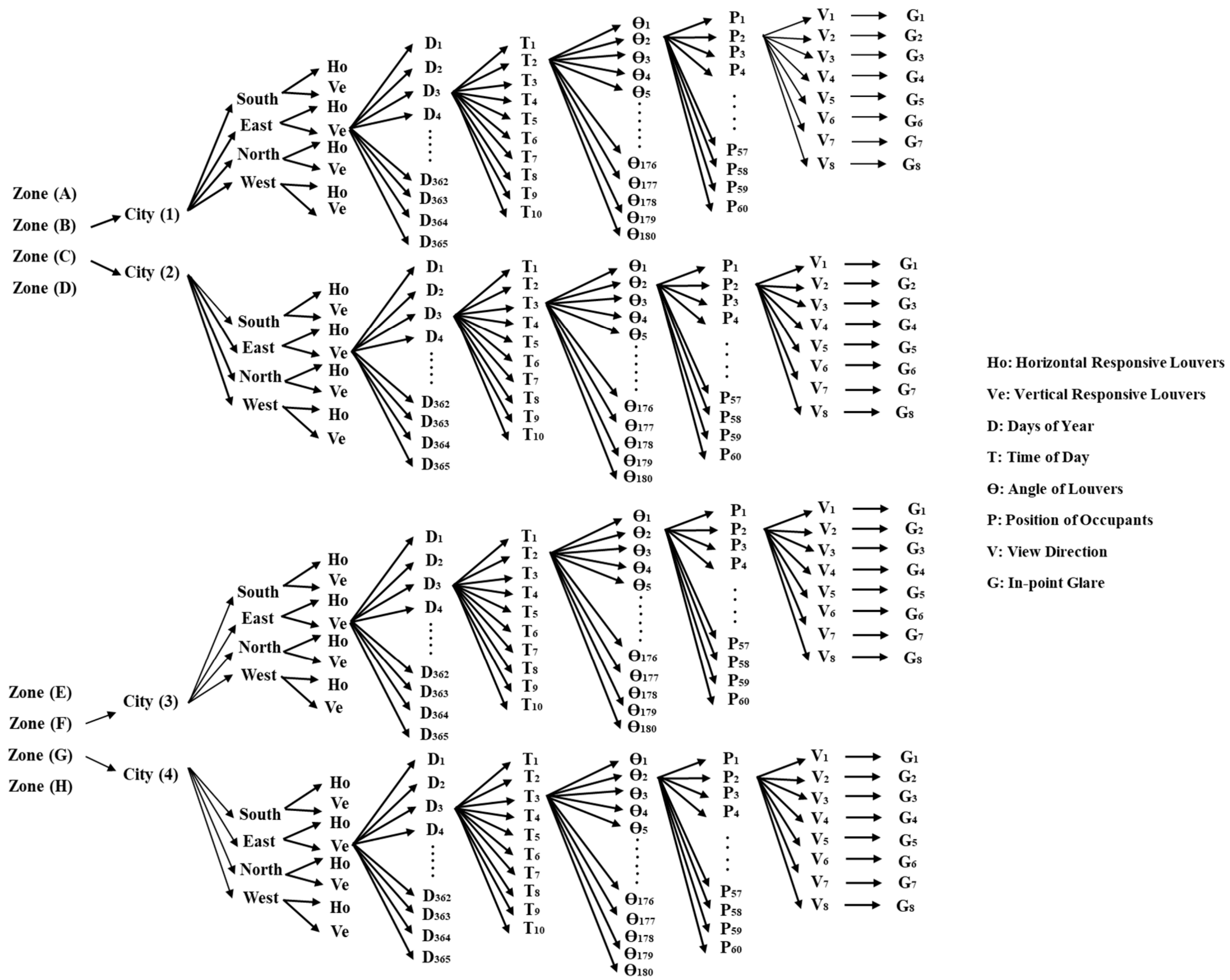

Figure 2. The flow and execution of data in the simulation process.

As shown in Figures 3–18, the fish-eye images illustrate the occupant views generated using the DIVA plugin in Grasshopper at two positions, A and B. It needs to be mentioned that the probability values (DGPs) have been converted to percentages (%) for better presentation. Figures 3–10 show an assumed occupant view in point A and its related values of DGP during the 21st of every month of the year in the city of Phoenix while fixed horizontal and vertical louvers (scenario i) have been applied to the south facade of the simulated office room. These Figures show that discomfort glare occurs during the hours after sunrise and before sunset when the solar altitude is low, especially in October, November, December, January, and February. The worst performance with maximum glare occurred in November and December for fixed horizontal and vertical louvers. Due to the high solar intensity in Phoenix throughout the day, occupants may also experience discomfort glare during the midday hours in most months, except for May, June, and July, using fixed horizontal and vertical louvers. In addition, the occurrence of discomfort glare in winter and fall was higher than in summer and spring seasons, considering scenario i. This result is due to the difference in solar altitude between the cold and warm seasons. Also, these Figures demonstrate that employing fixed horizontal and vertical louvers results in a comfortable glare-free experience at point A for approximately 62% and 60% of the year, respectively. As a result, fixed horizontal louvers can perform slightly better compared to fixed vertical louvers at point A with 38% vs 39%.

Figures 11–18 depict the occupant view at point B, along with the corresponding DGP values on the 21st of each month in Phoenix. In these simulations, fixed horizontal and vertical louvers (scenario i) are applied to the south-facing wall of the office room. The assumed occupant is able to experience a comfortable situation with no glare from April to August at point B if fixed horizontal louvers have been implemented. In contrast, fixed vertical louvers can only provide no glare conditions in June at point B. Maximum discomfort glare conditions have been recorded in January for fixed horizontal louvers and in December for fixed vertical louvers.

The occupants can experience glare-free situations at point B for 64% and 56% of the year when fixed horizontal and vertical louvers have been deployed, respectively. As a result, fixed vertical louvers perform slightly less effectively than fixed horizontal louvers at point B, with performance ratings of 44% and 36%, respectively. DGP measurements taken at points A and B revealed the inefficiency of the fixed louvers. As a result, implementing a responsive facade with hourly angle adjustments, directed by the proposed objective function, could effectively reduce the average of DGP values in the room (scenario ii).

Considering scenario ii, DGPs in the center point of the office room (point G) are displayed in Figure 19 when the optimal angles for each hour were applied for horizontal responsive facades from 8:00 to 18:00 on the 21st of January until June in the cities of Miami, Phoenix, Boston, and Milwaukee. DGP values remain imperceptible when hourly optimal angles are set for horizontal louvers in all chosen cities on the 21st of the specified months (DGPs < 0.21).

Figure 20 shows DGP values in point G, while optimum vertical angles were set on responsive louvers from 8:00 to 18:00 on the 21st of January, February, March, April, May, and June in the cities of Miami, Phoenix, Boston, and Milwaukee. The degree of glare sensations is imperceptible by using hourly optimum angles in all selected cities on the 21st of the mentioned months (DGPs < 0.22). When DGP values were less than 0.10, strange behaviors were observed in the hourly optimum angles, which could result from low illuminance in the entire office room.

Phoenix: South-Horizontal-Fixed Louvers with Angle of Zero-Point A (Baseline)										
1/21										
Image	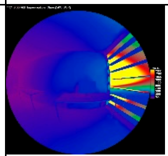	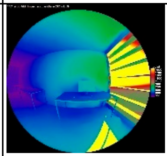	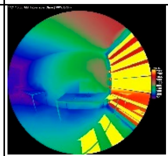	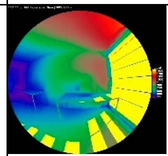	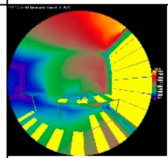	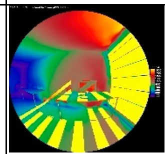	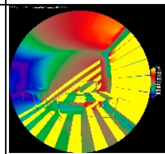	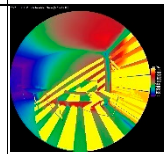	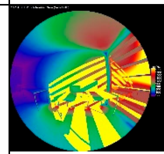	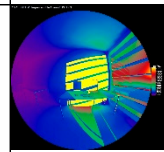
Time	8:00	9:00	10:00	11:00	12:00	13:00	14:00	15:00	16:00	17:00
DGPs	24% DGP	32% DGP	100% DGP	100% DGP	46% DGP	49% DGP	54% DGP	57% DGP	54% DGP	31% DGP
	Imperceptible	**Imperceptible**	**Intolerable**	**Intolerable**	**Intolerable**	**Intolerable**	**Intolerable**	**Intolerable**	**Intolerable**	**Imperceptible**
2/21										
Image	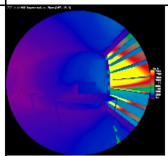	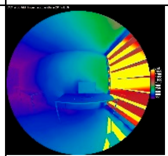	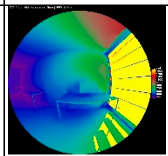	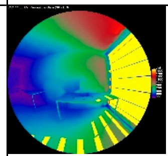	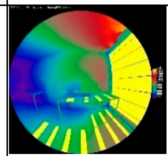	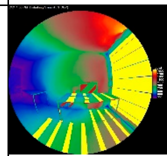	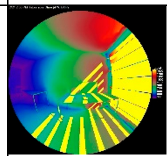	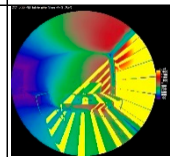	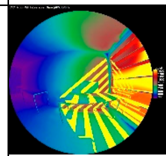	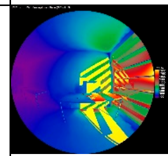
Time	8:00	9:00	10:00	11:00	12:00	13:00	14:00	15:00	16:00	17:00
DGPs	24% DGP	31% DGP	100% DGP	39% DGP	42% DGP	45% DGP	47% DGP	47% DGP	46% DGP	37% DGP
	Imperceptible	**Imperceptible**	**Intolerable**	**Perceptible**	**Disturbing**	**Disturbing**	**Intolerable**	**Intolerable**	**Intolerable**	**Perceptible**
3/21										
Image	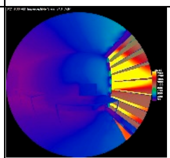	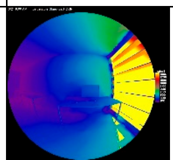	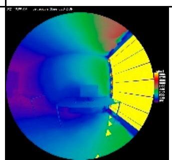	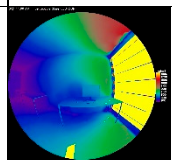	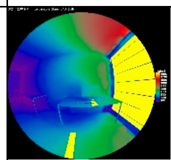	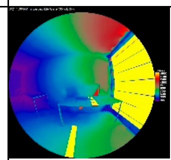	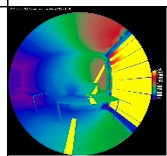	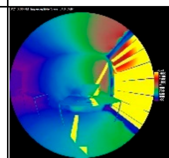	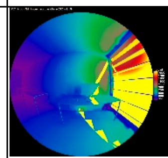	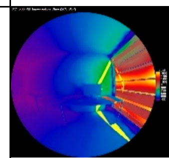
Time	8:00	9:00	10:00	11:00	12:00	13:00	14:00	15:00	16:00	17:00
DGPs	24% DGP	29% DGP	32% DGP	33% DGP	34% DGP	36% DGP	36% DGP	34% DGP	32% DGP	26% DGP
	Imperceptible	**Imperceptible**	**Imperceptible**	**Imperceptible**	**Imperceptible**	**Perceptible**	**Perceptible**	**Imperceptible**	**Imperceptible**	**Imperceptible**

Figure 3. Phoenix: south-horizontal-fixed louvers with the angle of zero-point A (Baseline).

Phoenix: South-Horizontal-Fixed Louvers with Angle of Zero-Point A (Baseline)										
4/21										
Image	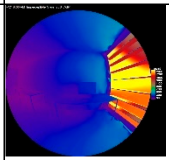	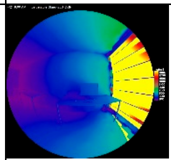	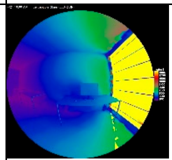	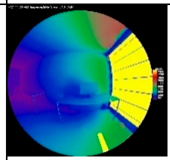	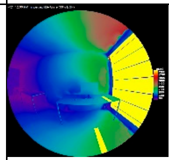	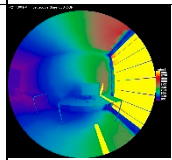	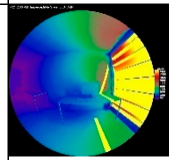	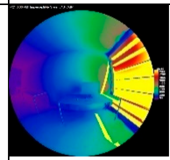	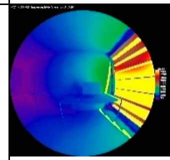	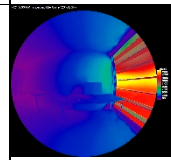
Time	8:00	9:00	10:00	11:00	12:00	13:00	14:00	15:00	16:00	17:00
DGPs	25% DGP	28% DGP	30% DGP	31% DGP	35% DGP	35% DGP	33% DGP	31% DGP	27% DGP	23% DGP
	Imperceptible	**Imperceptible**	**Imperceptible**	**Imperceptible**	**Perceptible**	**Perceptible**	**Imperceptible**	**Imperceptible**	**Imperceptible**	**Imperceptible**
5/21										
Image	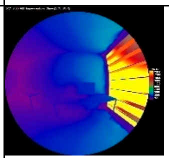	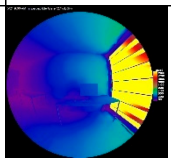	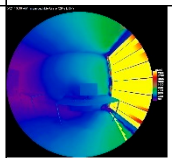	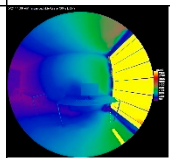	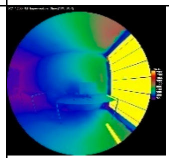	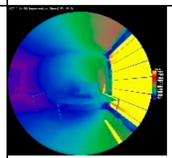	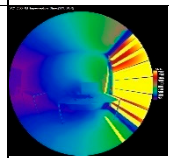	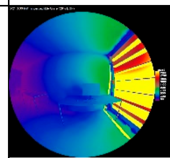	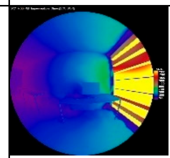	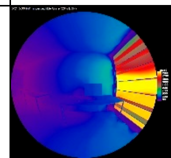
Time	8:00	9:00	10:00	11:00	12:00	13:00	14:00	15:00	16:00	17:00
DGPs	25% DGP	27% DGP	28% DGP	30% DGP	31% DGP	31% DGP	30% DGP	28% DGP	25% DGP	23% DGP
	Imperceptible	**Imperceptible**	**Imperceptible**	**Imperceptible**	**Imperceptible**	**Imperceptible**	**Imperceptible**	**Imperceptible**	**Imperceptible**	**Imperceptible**
6/21										
Image	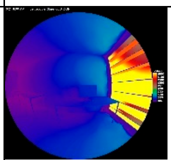	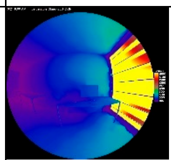	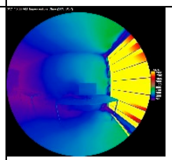	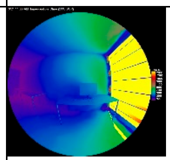	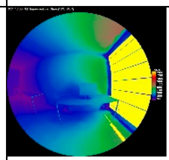	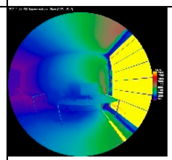	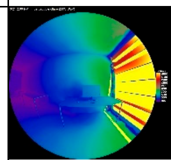	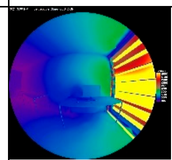	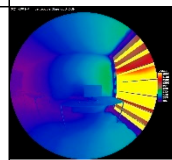	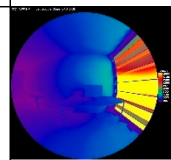
Time	8:00	9:00	10:00	11:00	12:00	13:00	14:00	15:00	16:00	17:00
DGPs	25% DGP	26% DGP	28% DGP	29% DGP	31% DGP	31% DGP	29% DGP	28% DGP	25% DGP	24% DGP
	Imperceptible	**Imperceptible**	**Imperceptible**	**Imperceptible**	**Imperceptible**	**Imperceptible**	**Imperceptible**	**Imperceptible**	**Imperceptible**	**Imperceptible**

Figure 4. Phoenix: south-horizontal-fixed louvers with the angle of zero-point A (Baseline).

Phoenix: South-Horizontal-Fixed Louvers with Angle of Zero-Point A (Baseline)										
7/21										
Image	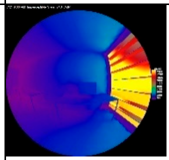	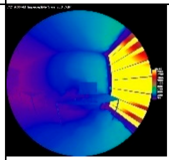	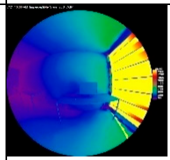	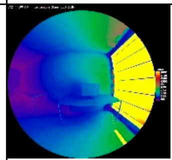	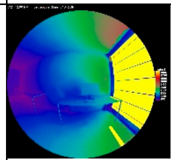	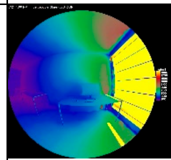	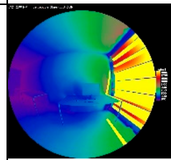	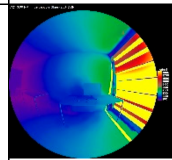	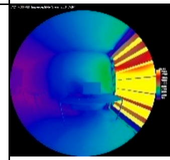	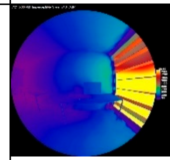
Time	8:00	9:00	10:00	11:00	12:00	13:00	14:00	15:00	16:00	17:00
DGPs	24% DGP	26% DGP	28% DGP	30% DGP	31% DGP	32% DGP	30% DGP	28% DGP	26% DGP	24% DGP
	Imperceptible	**Imperceptible**	**Imperceptible**	**Imperceptible**	**Imperceptible**	**Imperceptible**	**Imperceptible**	**Imperceptible**	**Imperceptible**	**Imperceptible**
8/21										
Image	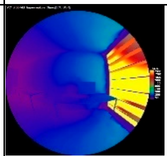	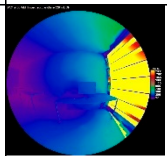	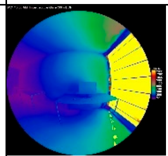	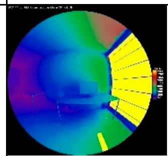	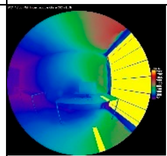	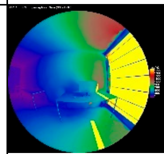	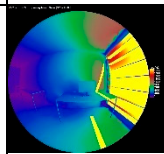	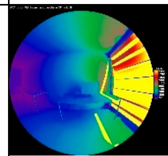	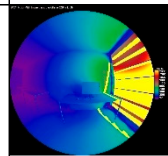	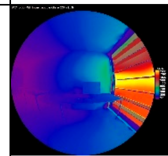
Time	8:00	9:00	10:00	11:00	12:00	13:00	14:00	15:00	16:00	17:00
DGPs	25% DGP	28% DGP	30% DGP	31% DGP	32% DGP	35% DGP	32% DGP	31% DGP	28% DGP	23% DGP
	Imperceptible	**Imperceptible**	**Imperceptible**	**Imperceptible**	**Imperceptible**	**Perceptible**	**Imperceptible**	**Imperceptible**	**Imperceptible**	**Imperceptible**
9/21										
Image	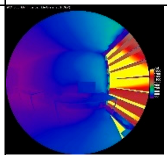	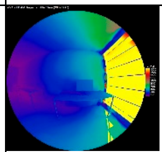	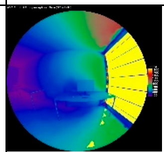	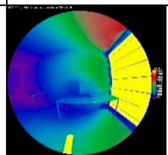	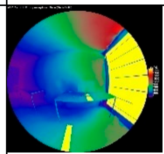	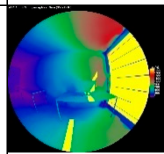	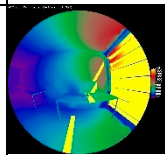	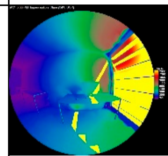	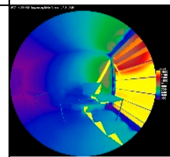	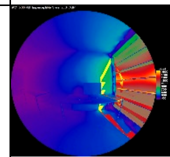
Time	8:00	9:00	10:00	11:00	12:00	13:00	14:00	15:00	16:00	17:00
DGPs	26% DGP	30% DGP	32% DGP	33% DGP	34% DGP	35% DGP	35% DGP	34% DGP	31% DGP	25% DGP
	Imperceptible	**Imperceptible**	**Imperceptible**	**Imperceptible**	**Imperceptible**	**Perceptible**	**Perceptible**	**Imperceptible**	**Imperceptible**	**Imperceptible**

Figure 5. Phoenix: south-horizontal-fixed louvers with the angle of zero-point A (Baseline).

Phoenix: South-Horizontal-Fixed Louvers with Angle of Zero-Point A (Baseline)										
10/21										
Image	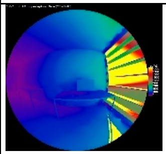	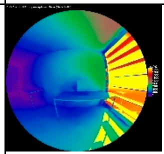	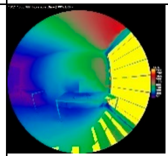	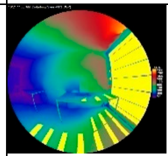	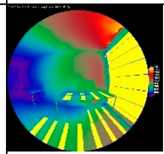	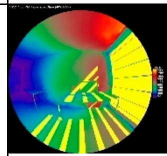	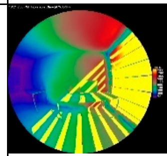	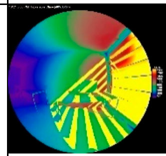	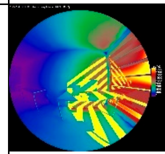	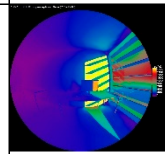
Time	8:00	9:00	10:00	11:00	12:00	13:00	14:00	15:00	16:00	17:00
DGPs	27% DGP	34% DGP	100% DGP	41% DGP	44% DGP	46% DGP	47% DGP	48% DGP	44% DGP	27% DGP
	Imperceptible	**Imperceptible**	**Intolerable**	**Disturbing**	**Disturbing**	**Intolerable**	**Intolerable**	**Intolerable**	**Disturbing**	**Imperceptible**
11/21										
Image	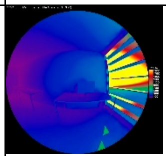	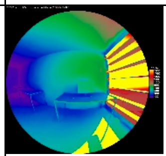	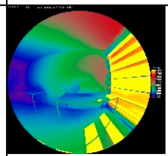	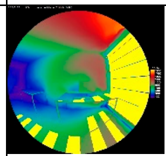	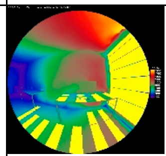	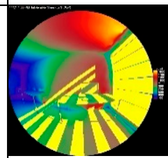	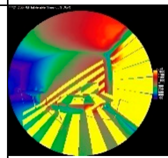	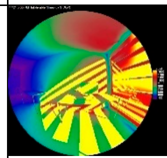	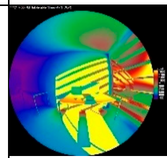	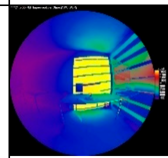
Time	8:00	9:00	10:00	11:00	12:00	13:00	14:00	15:00	16:00	17:00
DGPs	26% DGP	100% DGP	100% DGP	100% DGP	47% DGP	52% DGP	56% DGP	57% DGP	47% DGP	31% DGP
	Imperceptible	**Intolerable**	**Intolerable**	**Intolerable**	**Intolerable**	**Intolerable**	**Intolerable**	**Intolerable**	**Intolerable**	**Imperceptible**
12/21										
Image	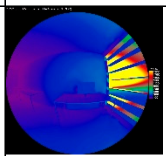	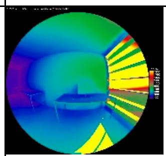	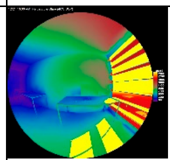	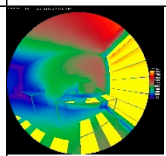	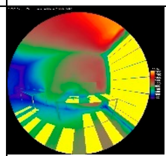	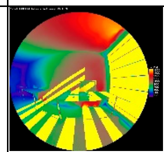	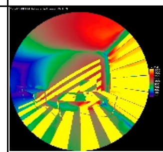	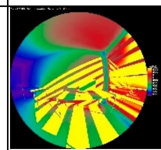	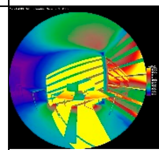	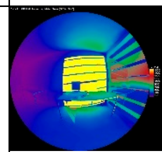
Time	8:00	9:00	10:00	11:00	12:00	13:00	14:00	15:00	16:00	17:00
DGPs	25% DGP	100% DGP	40% DGP	100% DGP	100% DGP	51% DGP	57% DGP	59% DGP	50% DGP	35% DGP
	Imperceptible	**Intolerable**	**Perceptible**	**Intolerable**	**Intolerable**	**Intolerable**	**Intolerable**	**Intolerable**	**Intolerable**	**Intolerable**

Figure 6. Phoenix: south-horizontal-fixed louvers with the angle of zero-point A (Baseline).

Phoenix: South-Vertical-Fixed Louvers with Angle of Zero-Point A (Baseline)										
1/21										
Image	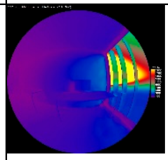	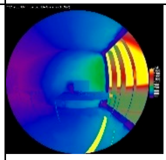	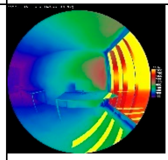	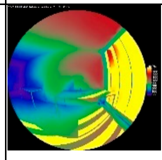	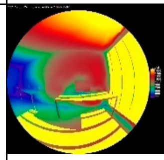	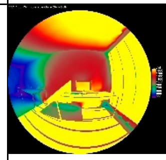	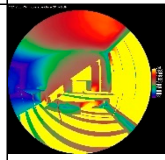	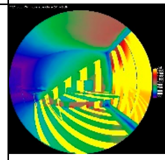	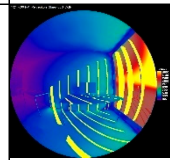	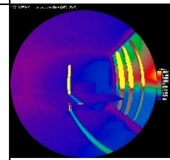
Time	8:00	9:00	10:00	11:00	12:00	13:00	14:00	15:00	16:00	17:00
DGPs	21% DGP	27% DGP	34% DGP	100% DGP	100% DGP	64% DGP	61% DGP	51% DGP	36% DGP	24% DGP
	Imperceptible	**Imperceptible**	**Imperceptible**	**Intolerable**	**Intolerable**	**Intolerable**	**Intolerable**	**Intolerable**	**Perceptible**	**Imperceptible**
2/21										
Image	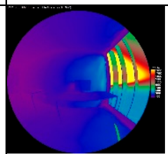	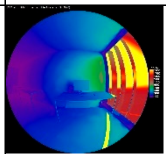	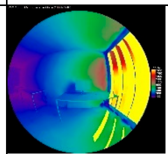	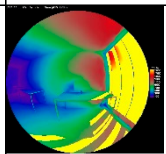	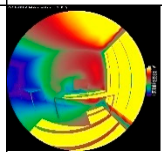	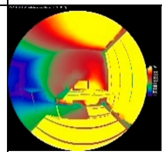	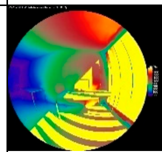	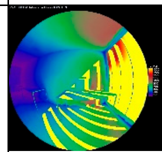	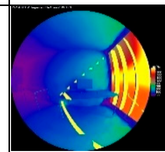	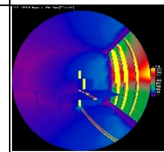
Time	8:00	9:00	10:00	11:00	12:00	13:00	14:00	15:00	16:00	17:00
DGPs	22% DGP	28% DGP	100% DGP	41% DGP	53% DGP	63% DGP	56% DGP	100% DGP	31% DGP	27% DGP
	Imperceptible	**Imperceptible**	**Intolerable**	**Disturbing**	**Intolerable**	**Intolerable**	**Intolerable**	**Intolerable**	**Imperceptible**	**Imperceptible**
3/21										
Image	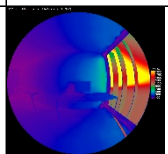	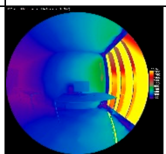	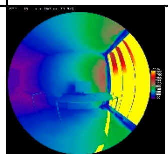	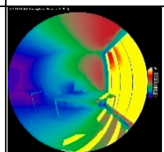	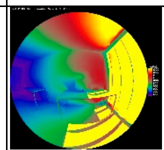	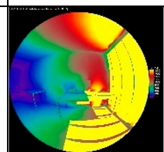	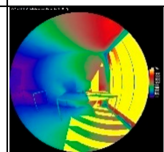	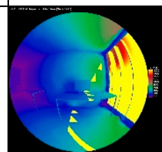	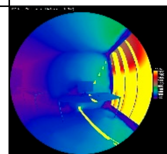	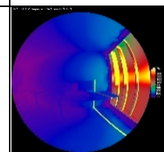
Time	8:00	9:00	10:00	11:00	12:00	13:00	14:00	15:00	16:00	17:00
DGPs	23% DGP	28% DGP	31% DGP	37% DGP	48% DGP	52% DGP	47% DGP	35% DGP	30% DGP	25% DGP
	Imperceptible	**Imperceptible**	**Imperceptible**	**Perceptible**	**Intolerable**	**Intolerable**	**Intolerable**	**Perceptible**	**Imperceptible**	**Imperceptible**

Figure 7. Phoenix: south-vertical-fixed louvers with the angle of zero-point A (Baseline).

Phoenix: South-Vertical-Fixed Louvers with Angle of Zero-Point A (Baseline)										
4/21										
Image	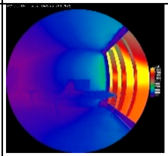	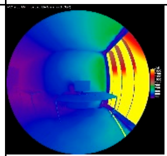	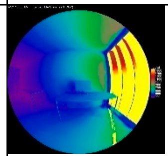	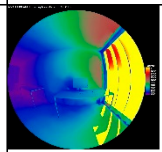	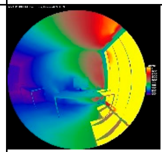	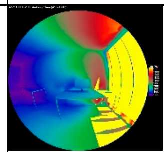	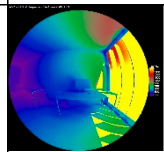	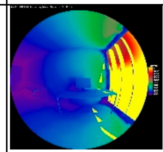	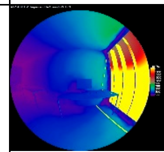	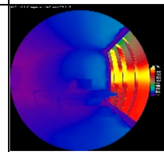
Time	8:00	9:00	10:00	11:00	12:00	13:00	14:00	15:00	16:00	17:00
DGPs	24% DGP	27% DGP	29% DGP	36% DGP	40% DGP	41% DGP	34% DGP	30% DGP	27% DGP	23% DGP
	Imperceptible	Imperceptible	Imperceptible	Perceptible	Disturbing	Disturbing	Imperceptible	Imperceptible	Imperceptible	Imperceptible
5/21										
Image	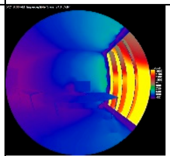	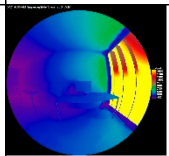	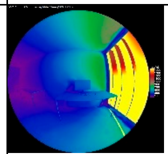	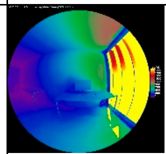	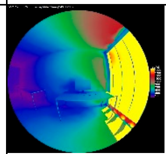	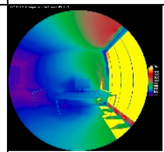	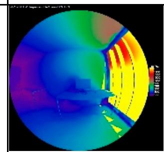	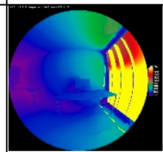	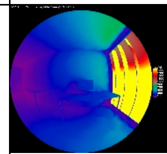	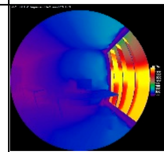
Time	8:00	9:00	10:00	11:00	12:00	13:00	14:00	15:00	16:00	17:00
DGPs	24% DGP	26% DGP	28% DGP	30% DGP	34% DGP	34% DGP	30% DGP	28% DGP	25% DGP	23% DGP
	Imperceptible	Imperceptible	Imperceptible	Imperceptible	Imperceptible	Imperceptible	Imperceptible	Imperceptible	Imperceptible	Imperceptible
6/21										
Image	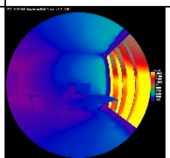	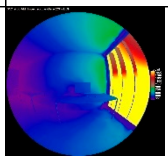	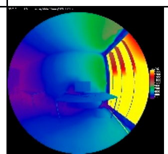	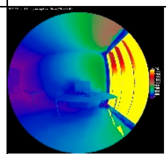	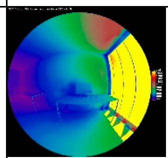	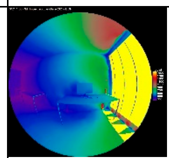	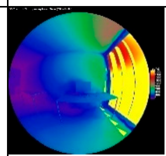	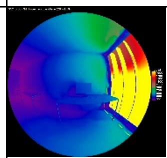	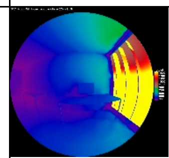	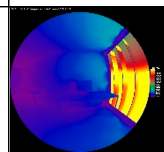
Time	8:00	9:00	10:00	11:00	12:00	13:00	14:00	15:00	16:00	17:00
DGPs	24% DGP	26% DGP	28% DGP	29% DGP	32% DGP	32% DGP	29% DGP	28% DGP	25% DGP	23% DGP
	Imperceptible	Imperceptible	Imperceptible	Imperceptible	Imperceptible	Imperceptible	Imperceptible	Imperceptible	Imperceptible	Imperceptible

Figure 8. Phoenix: south-vertical-fixed louvers with the angle of zero-point A (Baseline).

Phoenix: South-Vertical-Fixed Louvers with Angle of Zero-Point A (Baseline)										
7/21										
Image	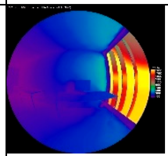	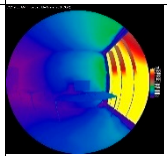	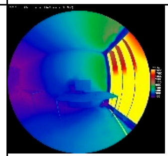	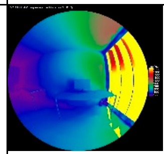	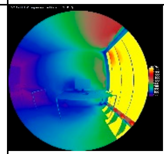	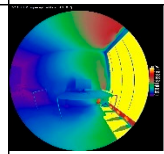	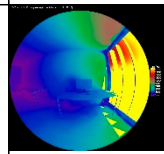	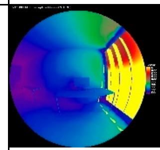	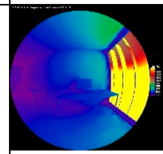	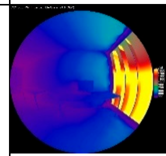
Time	8:00	9:00	10:00	11:00	12:00	13:00	14:00	15:00	16:00	17:00
DGPs	24% DGP	26% DGP	28% DGP	29% DGP	33% DGP	34% DGP	30% DGP	28% DGP	26% DGP	24% DGP
	Imperceptible	**Imperceptible**	**Imperceptible**	**Imperceptible**	**Imperceptible**	**Imperceptible**	**Imperceptible**	**Imperceptible**	**Imperceptible**	**Imperceptible**
8/21										
Image	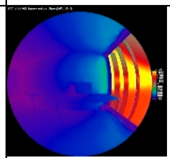	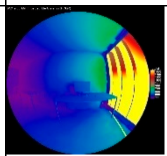	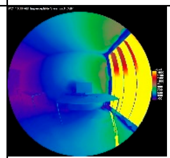	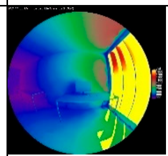	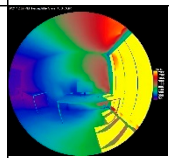	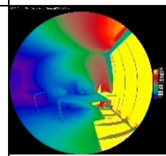	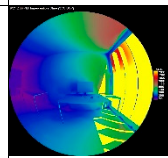	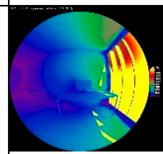	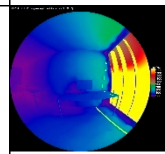	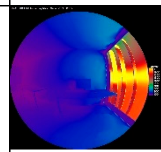
Time	8:00	9:00	10:00	11:00	12:00	13:00	14:00	15:00	16:00	17:00
DGPs	24% DGP	27% DGP	29% DGP	32% DGP	40% DGP	42% DGP	36% DGP	31% DGP	27% DGP	23% DGP
	Imperceptible	**Imperceptible**	**Imperceptible**	**Imperceptible**	**Perceptible**	**Disturbing**	**Perceptible**	**Imperceptible**	**Imperceptible**	**Imperceptible**
9/21										
Image	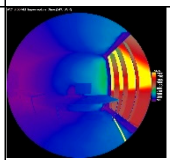	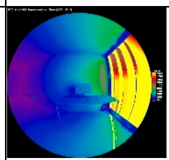	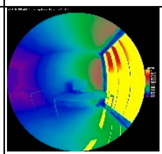	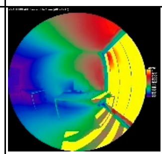	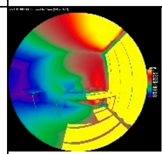	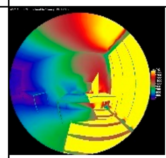	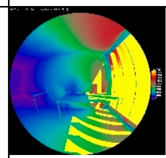	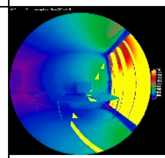	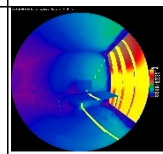	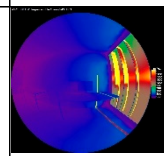
Time	8:00	9:00	10:00	11:00	12:00	13:00	14:00	15:00	16:00	17:00
DGPs	24% DGP	28% DGP	32% DGP	40% DGP	50% DGP	51% DGP	44% DGP	32% DGP	28% DGP	24% DGP
	Imperceptible	**Imperceptible**	**Imperceptible**	**Perceptible**	**Intolerable**	**Intolerable**	**Disturbing**	**Imperceptible**	**Imperceptible**	**Imperceptible**

Figure 9. Phoenix: south-vertical-fixed louvers with the angle of zero-point A (Baseline).

Phoenix: South-Vertical-Fixed Louvers with Angle of Zero-Point A (Baseline)										
10/21										
Image	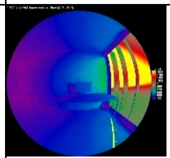	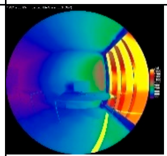	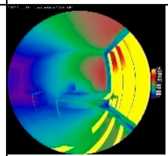	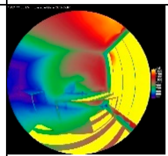	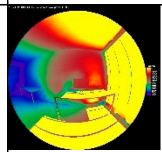	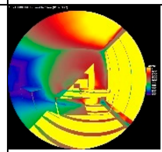	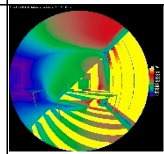	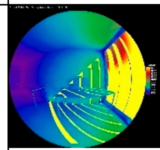	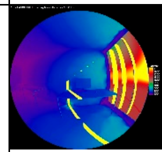	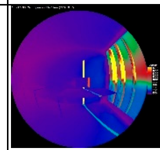
Time	8:00	9:00	10:00	11:00	12:00	13:00	14:00	15:00	16:00	17:00
DGPs	25% DGP	30% DGP	100% DGP	67% DGP	61% DGP	61% DGP	100% DGP	38% DGP	29% DGP	22% DGP
	Imperceptible	**Imperceptible**	**Intolerable**	**Intolerable**	**Intolerable**	**Intolerable**	**Intolerable**	**Perceptible**	**Imperceptible**	**Imperceptible**
11/21										
Image	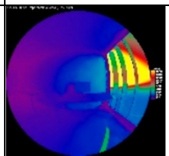	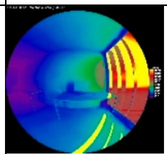	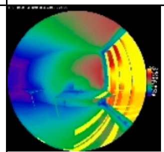	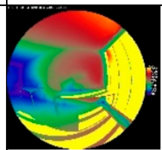	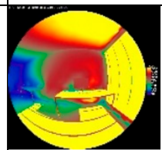	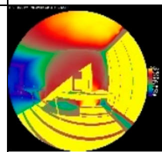	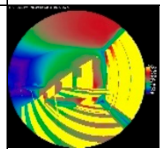	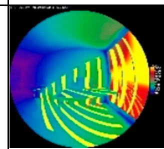	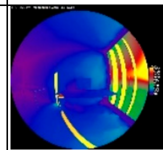	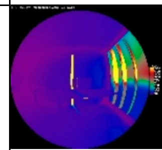
Time	8:00	9:00	10:00	11:00	12:00	13:00	14:00	15:00	16:00	17:00
DGPs	23% DGP	100% DGP	100% DGP	100% DGP	100% DGP	64% DGP	100% DGP	45% DGP	28% DGP	27% DGP
	Imperceptible	**Intolerable**	**Intolerable**	**Intolerable**	**Intolerable**	**Intolerable**	**Intolerable**	**Intolerable**	**Imperceptible**	**Imperceptible**
12/21										
Image	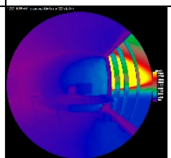	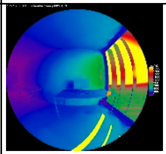	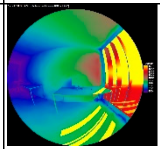	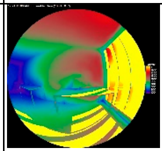	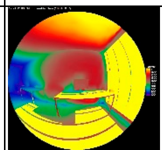	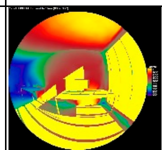	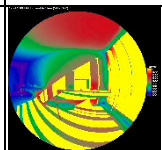	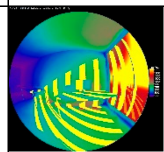	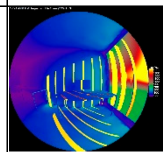	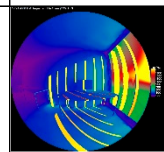
Time	8:00	9:00	10:00	11:00	12:00	13:00	14:00	15:00	16:00	17:00
DGPs	22% DGP	100% DGP	100% DGP	100% DGP	100% DGP	63% DGP	59% DGP	49% DGP	33% DGP	23% DGP
	Imperceptible	**Intolerable**	**Intolerable**	**Intolerable**	**Intolerable**	**Intolerable**	**Intolerable**	**Intolerable**	**Imperceptible**	**Imperceptible**

Figure 10. Phoenix: south-vertical-fixed louvers with the angle of zero-point A (Baseline).

Phoenix: South-Horizontal-Fixed Louvers with Angle of Zero-Point B (Baseline)										
1/21										
Image	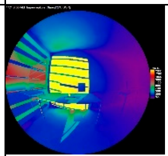	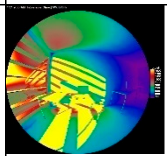	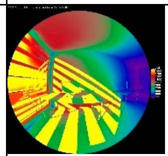	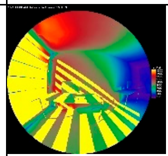	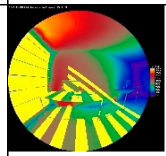	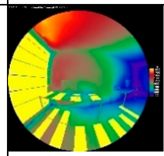	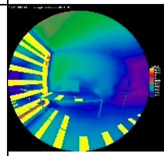	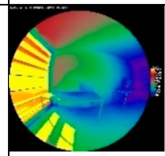	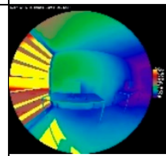	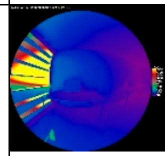
Time	8:00	9:00	10:00	11:00	12:00	13:00	14:00	15:00	16:00	17:00
DGPs	36% DGP	50% DGP	57% DGP	55% DGP	51% DGP	47% DGP	100% DGP	100% DGP	100% DGP	25% DGP
	Perceptible	**Intolerable**	**Intolerable**	**Intolerable**	**Intolerable**	**Intolerable**	**Intolerable**	**Intolerable**	**Intolerable**	**Imperceptible**
2/21										
Image	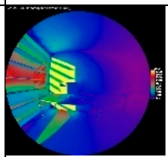	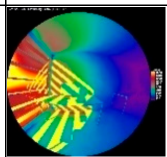	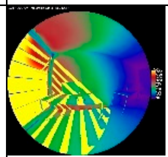	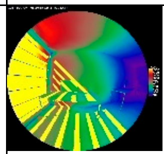	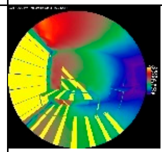	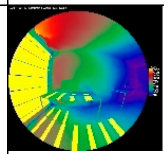	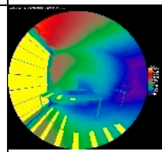	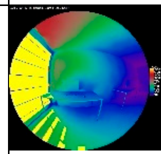	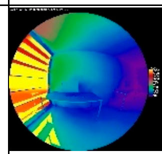	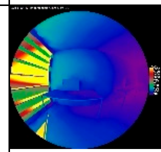
Time	8:00	9:00	10:00	11:00	12:00	13:00	14:00	15:00	16:00	17:00
DGPs	29% DGP	44% DGP	48% DGP	46% DGP	46% DGP	43% DGP	40% DGP	100% DGP	33% DGP	26% DGP
	Imperceptible	**Disturbing**	**Intolerable**	**Intolerable**	**Intolerable**	**Disturbing**	**Perceptible**	**Intolerable**	**Imperceptible**	**Imperceptible**
3/21										
Image	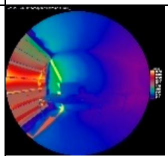	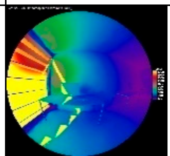	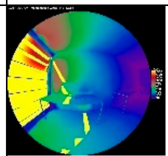	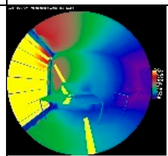	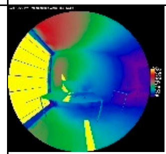	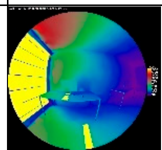	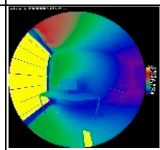	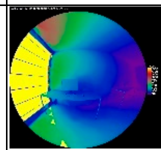	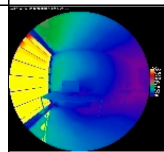	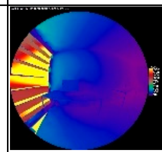
Time	8:00	9:00	10:00	11:00	12:00	13:00	14:00	15:00	16:00	17:00
DGPs	25% DGP	31% DGP	34% DGP	35% DGP	36% DGP	34% DGP	33% DGP	32% DGP	29% DGP	25% DGP
9	**Imperceptible**	**Imperceptible**	**Imperceptible**	**Imperceptible**	**Perceptible**	**Imperceptible**	**Imperceptible**	**Imperceptible**	**Imperceptible**	**Imperceptible**

Figure 11. Phoenix: south-horizontal-fixed louvers with the angle of zero-point B (Baseline).

Phoenix: South-Horizontal-Fixed Louvers with Angle of Zero-Point B (Baseline)										
4/21										
Image	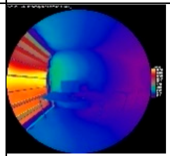	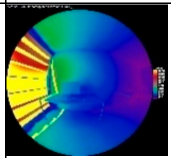	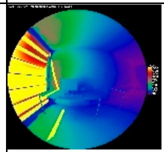	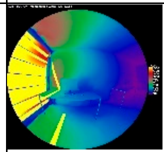	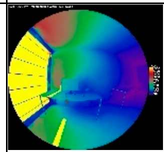	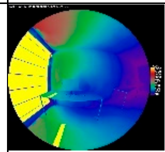	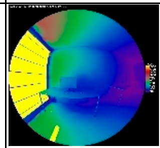	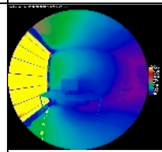	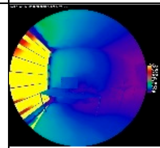	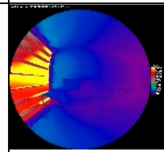
Time	8:00	9:00	10:00	11:00	12:00	13:00	14:00	15:00	16:00	17:00
DGPs	23% DGP	28% DGP	31% DGP	32% DGP	33% DGP	32% DGP	31% DGP	29% DGP	27% DGP	24% DGP
100%	**Imperceptible**	**Imperceptible**	**Imperceptible**	**Imperceptible**	**Imperceptible**	**Imperceptible**	**Imperceptible**	**Imperceptible**	**Imperceptible**	**Imperceptible**
5/21										
Image	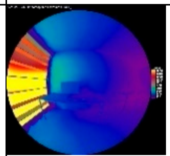	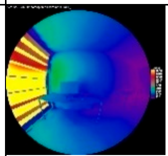	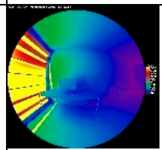	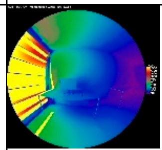	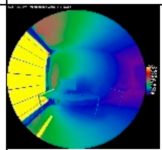	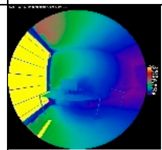	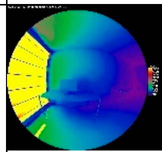	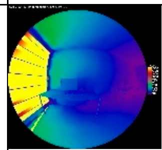	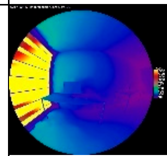	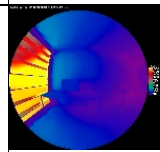
Time	8:00	9:00	10:00	11:00	12:00	13:00	14:00	15:00	16:00	17:00
DGPs	24% DGP	26% DGP	28% DGP	30% DGP	31% DGP	31% DGP	29% DGP	28% DGP	26% DGP	24% DGP
100%	**Imperceptible**	**Imperceptible**	**Imperceptible**	**Imperceptible**	**Imperceptible**	**Imperceptible**	**Imperceptible**	**Imperceptible**	**Imperceptible**	**Imperceptible**
6/21										
Image	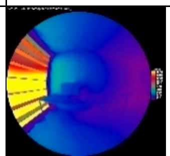	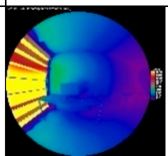	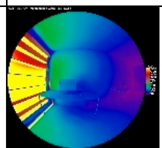	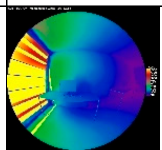	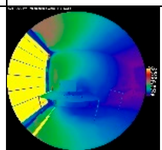	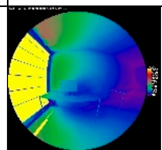	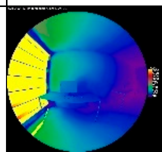	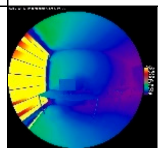	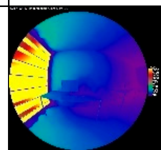	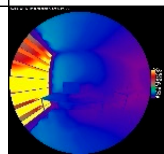
Time	8:00	9:00	10:00	11:00	12:00	13:00	14:00	15:00	16:00	17:00
DGPs	24% DGP	26% DGP	28% DGP	29% DGP	31% DGP	31% DGP	29% DGP	28% DGP	25% DGP	24% DGP
100%	**Imperceptible**	**Imperceptible**	**Imperceptible**	**Imperceptible**	**Imperceptible**	**Imperceptible**	**Imperceptible**	**Imperceptible**	**Imperceptible**	**Imperceptible**

Figure 12. Phoenix: south-horizontal-fixed louvers with the angle of zero-point B (Baseline).

Phoenix: South-Horizontal-Fixed Louvers with Angle of Zero-Point B (Baseline)										
7/21										
Image	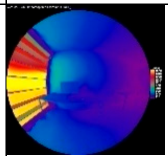	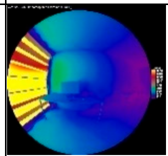	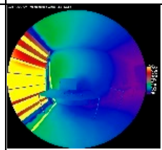	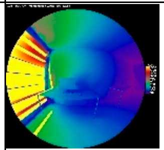	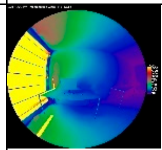	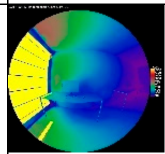	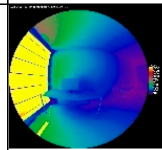	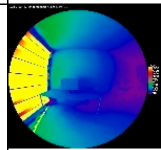	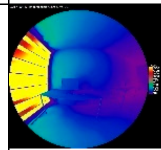	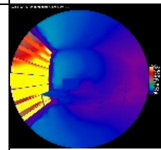
Time	8:00	9:00	10:00	11:00	12:00	13:00	14:00	15:00	16:00	17:00
DGPs	23% DGP	25% DGP	28% DGP	30% DGP	31% DGP	31% DGP	30% DGP	28% DGP	27% DGP	25% DGP
100%	**Imperceptible**	**Imperceptible**	**Imperceptible**	**Imperceptible**	**Imperceptible**	**Imperceptible**	**Imperceptible**	**Imperceptible**	**Imperceptible**	**Imperceptible**
8/21										
Image	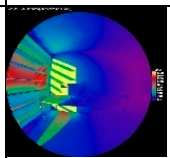	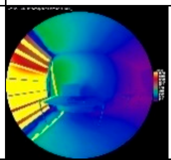	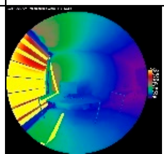	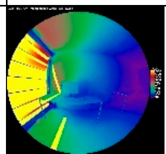	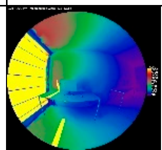	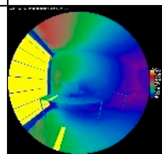	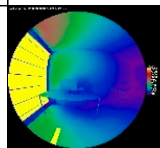	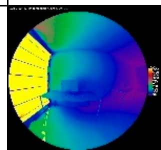	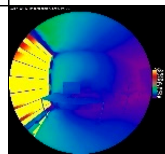	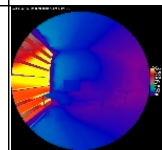
Time	8:00	9:00	10:00	11:00	12:00	13:00	14:00	15:00	16:00	17:00
DGPs	23% DGP	28% DGP	31% DGP	32% DGP	33% DGP	32% DGP	31% DGP	30% DGP	28% DGP	24% DGP
100%	**Imperceptible**	**Imperceptible**	**Imperceptible**	**Imperceptible**	**Imperceptible**	**Imperceptible**	**Imperceptible**	**Imperceptible**	**Imperceptible**	**Imperceptible**
9/21										
Image	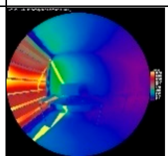	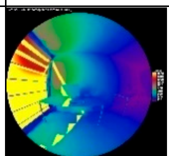	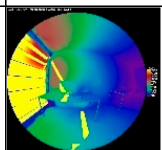	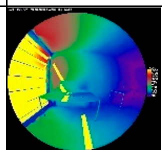	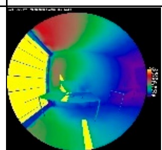	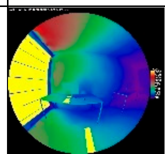	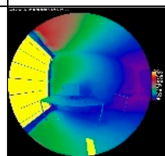	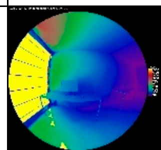	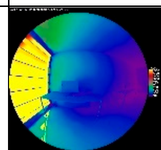	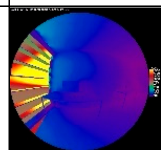
Time	8:00	9:00	10:00	11:00	12:00	13:00	14:00	15:00	16:00	17:00
DGPs	26% DGP	32% DGP	35% DGP	35% DGP	36% DGP	36% DGP	32% DGP	32% DGP	29% DGP	24% DGP
80%	**Imperceptible**	**Imperceptible**	**Imperceptible**	**Imperceptible**	**Perceptible**	**Perceptible**	**Imperceptible**	**Imperceptible**	**Imperceptible**	**Imperceptible**

Figure 13. Phoenix: south-vertical-fixed louvers with the angle of zero-point B (Baseline).

Phoenix: South-Horizontal-Fixed Louvers with Angle of Zero-Point B (Baseline)										
10/21										
Image	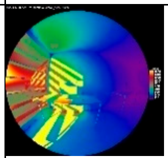	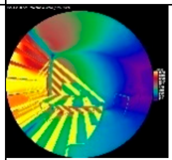	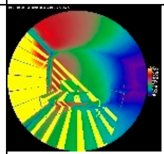	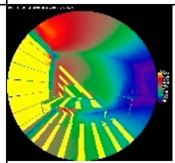	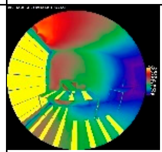	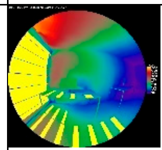	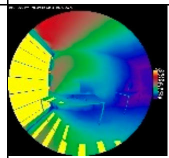	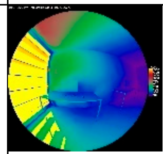	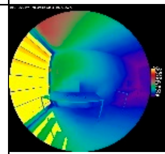	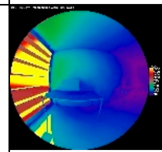
Time	8:00	9:00	10:00	11:00	12:00	13:00	14:00	15:00	16:00	17:00
DGPs	40% DGP	48% DGP	47% DGP	47% DGP	45% DGP	42% DGP	100% DGP	100% DGP	100% DGP	30% DGP
10%	**Intolerable**	**Intolerable**	**Intolerable**	**Intolerable**	**Disturbing**	**Disturbing**	**Intolerable**	**Intolerable**	**Intolerable**	**Imperceptible**
11/21										
Image	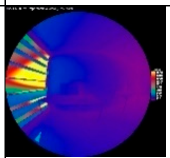	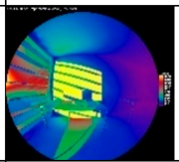	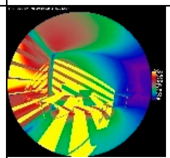	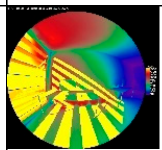	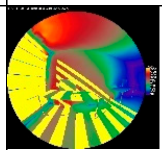	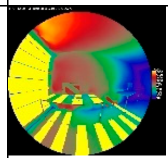	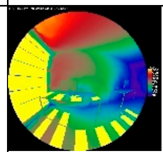	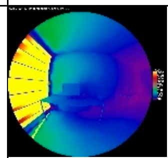	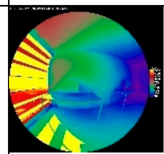	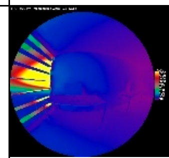
Time	8:00	9:00	10:00	11:00	12:00	13:00	14:00	15:00	16:00	17:00
DGPs	23% DGP	36% DGP	55% DGP	57% DGP	54% DGP	49% DGP	87% DGP	100% DGP	31% DGP	31% DGP
30%	**Imperceptible**	**Perceptible**	**Intolerable**	**Intolerable**	**Intolerable**	**Intolerable**	**Intolerable**	**Intolerable**	**Imperceptible**	**Imperceptible**
12/21										
Image	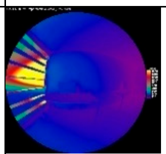	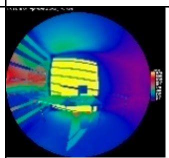	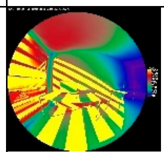	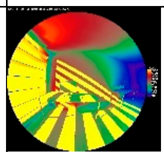	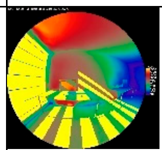	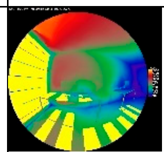	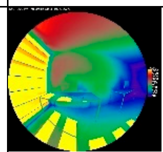	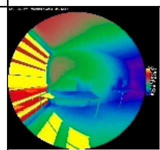	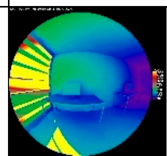	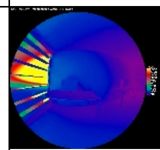
Time	8:00	9:00	10:00	11:00	12:00	13:00	14:00	15:00	16:00	17:00
DGPs	32% DGP	53% DGP	59% DGP	56% DGP	50% DGP	100% DGP	100% DGP	39% DGP	100% DGP	24% DGP
20%	**Imperceptible**	**Intolerable**	**Intolerable**	**Intolerable**	**Intolerable**	**Intolerable**	**Intolerable**	**Perceptible**	**Intolerable**	**Imperceptible**

Figure 14. Phoenix: south-vertical-fixed louvers with the angle of zero-point B (Baseline).

Phoenix: South-Vertical-Fixed Louvers with Angle of Zero-Point B (Baseline)										
1/21										
Image	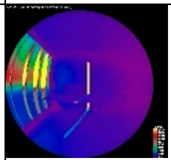	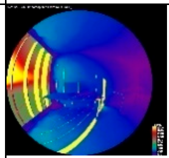	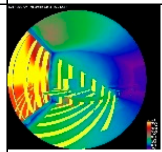	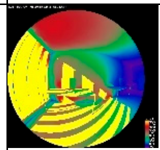	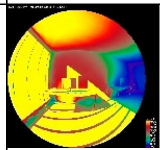	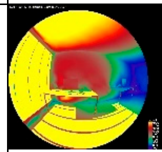	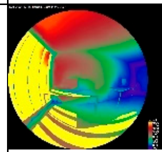	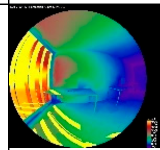	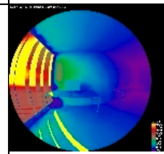	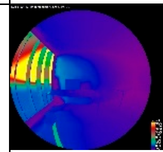
Time	8:00	9:00	10:00	11:00	12:00	13:00	14:00	15:00	16:00	17:00
DGPs	23% DGP	30% DGP	46% DGP	58% DGP	64% DGP	60% DGP	46% DGP	37% DGP	98% DGP	23% DGP
30%	**Imperceptible**	**Imperceptible**	**Intolerable**	**Intolerable**	**Intolerable**	**Intolerable**	**Intolerable**	**Perceptible**	**Intolerable**	**Imperceptible**
2/21										
Image	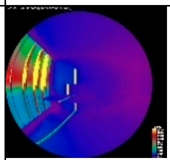	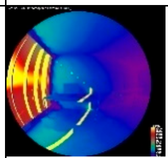	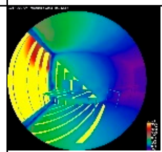	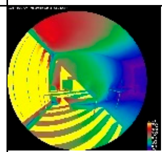	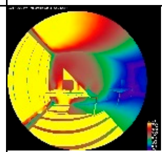	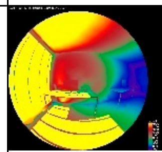	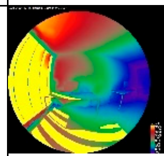	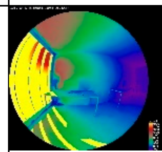	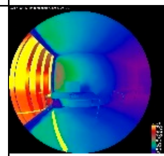	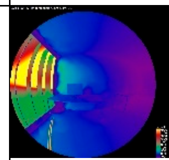
Time	8:00	9:00	10:00	11:00	12:00	13:00	14:00	15:00	16:00	17:00
DGPs	23% DGP	30% DGP	40% DGP	53% DGP	62% DGP	60% DGP	45% DGP	100% DGP	30% DGP	24% DGP
40%	**Imperceptible**	**Imperceptible**	**Perceptible**	**Intolerable**	**Intolerable**	**Intolerable**	**Intolerable**	**Intolerable**	**Imperceptible**	**Imperceptible**
3/21										
Image	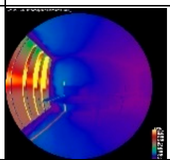	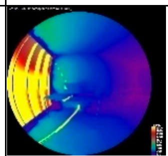	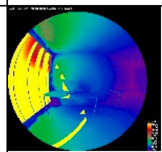	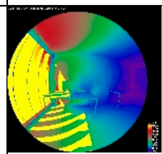	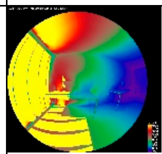	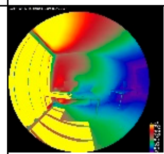	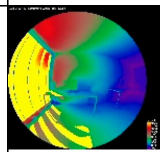	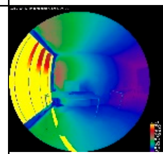	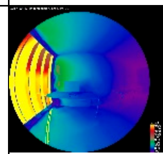	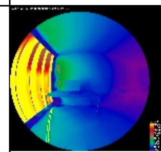
Time	8:00	9:00	10:00	11:00	12:00	13:00	14:00	15:00	16:00	17:00
DGPs	24% DGP	30% DGP	34% DGP	45% DGP	52% DGP	50% DGP	40% DGP	32% DGP	28% DGP	28% DGP
50%	**Imperceptible**	**Imperceptible**	**Imperceptible**	**Disturbing**	**Intolerable**	**Intolerable**	**Disturbing**	**Imperceptible**	**Imperceptible**	**Imperceptible**

Figure 15. Phoenix: south-vertical-fixed louvers with the angle of zero-point B (Baseline).

Phoenix: South-Vertical-Fixed Louvers with Angle of Zero-Point B (Baseline)										
4/21										
Image	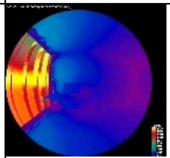	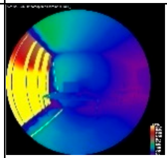	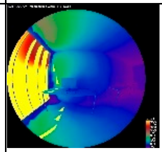	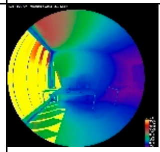	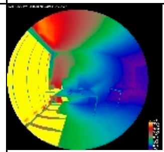	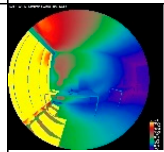	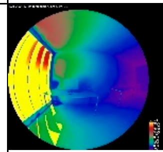	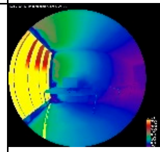	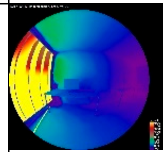	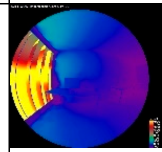
Time	8:00	9:00	10:00	11:00	12:00	13:00	14:00	15:00	16:00	17:00
DGPs	24% DGP	28% DGP	31% DGP	36% DGP	43% DGP	40% DGP	36% DGP	29% DGP	27% DGP	24% DGP
60%	**Imperceptible**	**Imperceptible**	**Imperceptible**	**Perceptible**	**Disturbing**	**Disturbing**	**Perceptible**	**Imperceptible**	**Imperceptible**	**Imperceptible**
5/21										
Image	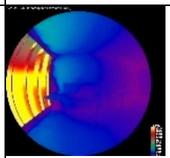	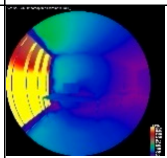	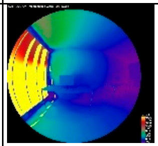	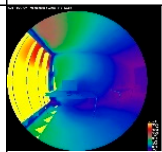	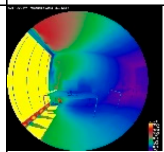	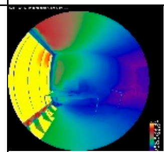	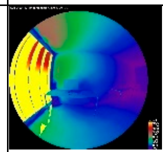	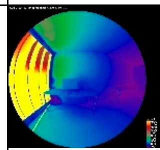	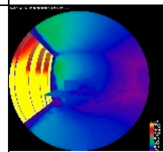	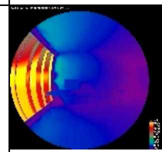
Time	8:00	9:00	10:00	11:00	12:00	13:00	14:00	15:00	16:00	17:00
DGPs	24% DGP	26% DGP	29% DGP	31% DGP	35% DGP	34% DGP	30% DGP	28% DGP	26% DGP	24% DGP
90%	**Imperceptible**	**Imperceptible**	**Imperceptible**	**Imperceptible**	**Perceptible**	**Imperceptible**	**Imperceptible**	**Imperceptible**	**Imperceptible**	**Imperceptible**
6/21										
Image	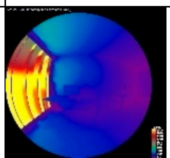	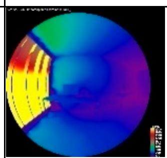	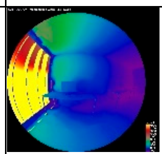	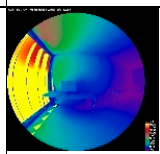	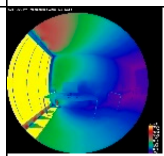	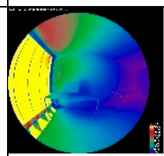	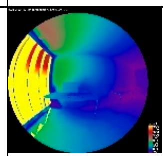	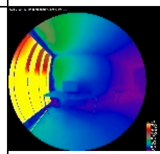	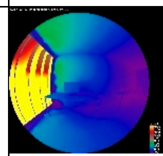	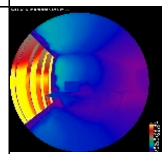
Time	8:00	9:00	10:00	11:00	12:00	13:00	14:00	15:00	16:00	17:00
DGPs	24% DGP	26% DGP	28% DGP	30% DGP	33% DGP	33% DGP	29% DGP	28% DGP	26% DGP	24% DGP
100%	**Imperceptible**	**Imperceptible**	**Imperceptible**	**Imperceptible**	**Imperceptible**	**Imperceptible**	**Imperceptible**	**Imperceptible**	**Imperceptible**	**Imperceptible**

Figure 16. Phoenix: south-vertical-fixed louvers with the angle of zero-point B (Baseline).

Phoenix: South-Vertical-Fixed Louvers with Angle of Zero-Point B (Baseline)										
7/21										
Image	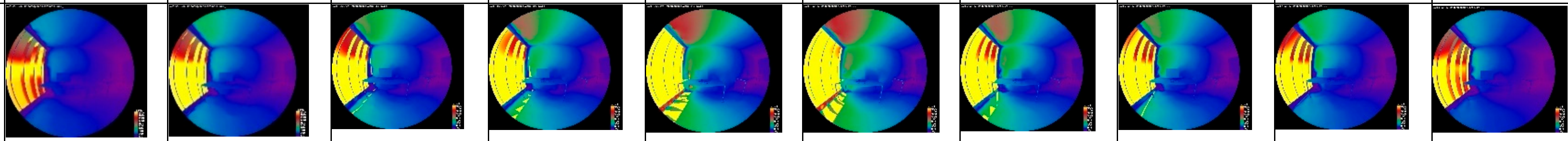									
Time	8:00	9:00	10:00	11:00	12:00	13:00	14:00	15:00	16:00	17:00
DGPs	24% DGP	26% DGP	28% DGP	30% DGP	34% DGP	36% DGP	30% DGP	28% DGP	26% DGP	24% DGP
90%	**Imperceptible**	**Imperceptible**	**Imperceptible**	**Imperceptible**	**Imperceptible**	**Perceptible**	**Imperceptible**	**Imperceptible**	**Imperceptible**	**Imperceptible**
8/21										
Image	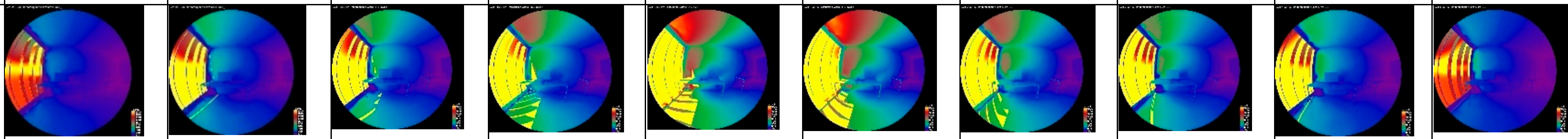									
Time	8:00	9:00	10:00	11:00	12:00	13:00	14:00	15:00	16:00	17:00
DGPs	24% DGP	27% DGP	31% DGP	36% DGP	42% DGP	41% DGP	33% DGP	30% DGP	27% DGP	24% DGP
70%	**Imperceptible**	**Imperceptible**	**Imperceptible**	**Perceptible**	**Disturbing**	**Disturbing**	**Imperceptible**	**Imperceptible**	**Imperceptible**	**Imperceptible**
9/21										
Image	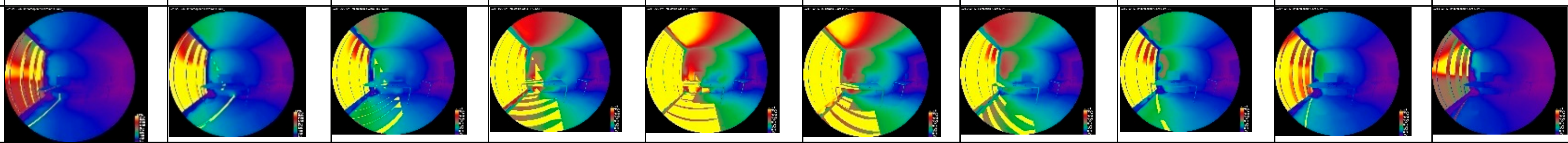									
Time	8:00	9:00	10:00	11:00	12:00	13:00	14:00	15:00	16:00	17:00
DGPs	25% DGP	31% DGP	36% DGP	47% DGP	54% DGP	49% DGP	38% DGP	31% DGP	28% DGP	23% DGP
50%	**Imperceptible**	**Imperceptible**	**Perceptible**	**Intolerable**	**Intolerable**	**Intolerable**	**Perceptible**	**Imperceptible**	**Imperceptible**	**Imperceptible**

Figure 17. Phoenix: south-vertical-fixed louvers with the angle of zero-point B (Baseline).

Phoenix: South-Vertical-Fixed Louvers with Angle of Zero-Point B (Baseline)										
10/21										
Image	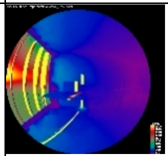	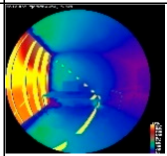	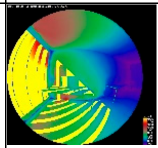	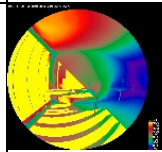	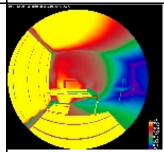	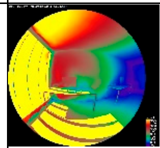	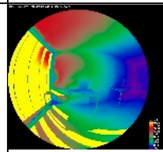	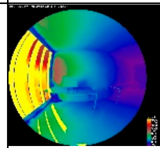	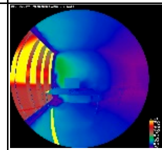	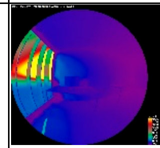
Time	8:00	9:00	10:00	11:00	12:00	13:00	14:00	15:00	16:00	17:00
DGPs	28% DGP	32% DGP	47% DGP	58% DGP	64% DGP	53% DGP	100% DGP	61% DGP	27% DGP	21% DGP
40%	**Imperceptible**	**Imperceptible**	**Intolerable**	**Intolerable**	**Intolerable**	**Intolerable**	**Intolerable**	**Intolerable**	**Imperceptible**	**Imperceptible**
11/21										
Image	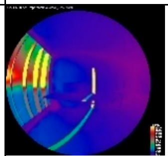	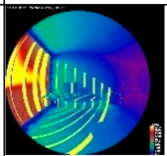	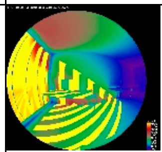	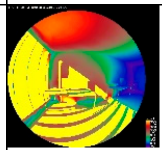	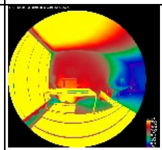	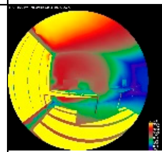	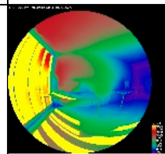	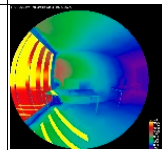	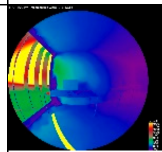	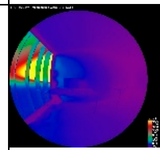
Time	8:00	9:00	10:00	11:00	12:00	13:00	14:00	15:00	16:00	17:00
DGPs	21% DGP	100% DGP	52% DGP	100% DGP	65% DGP	100% DGP	100% DGP	100% DGP	27% DGP	21% DGP
30%	**Imperceptible**	**Intolerable**	**Intolerable**	**Intolerable**	**Intolerable**	**Intolerable**	**Intolerable**	**Intolerable**	**Imperceptible**	**Imperceptible**
12/21										
Image	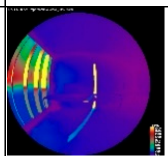	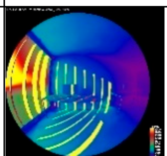	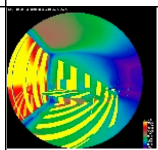	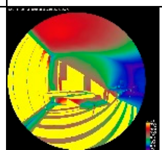	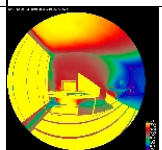	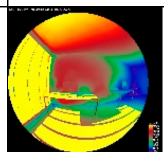	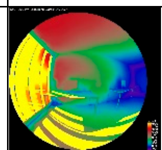	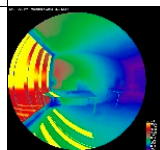	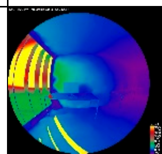	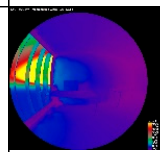
Time	8:00	9:00	10:00	11:00	12:00	13:00	14:00	15:00	16:00	17:00
DGPs	24% DGP	36% DGP	50% DGP	60% DGP	63% DGP	100% DGP	43% DGP	36% DGP	52% DGP	22% DGP
20%	**Imperceptible**	**Perceptible**	**Intolerable**	**Intolerable**	**Intolerable**	**Intolerable**	**Disturbing**	**Perceptible**	**Intolerable**	**Imperceptible**

Figure 18. Phoenix: south-vertical-fixed louvers with the angle of zero-point B (Baseline).

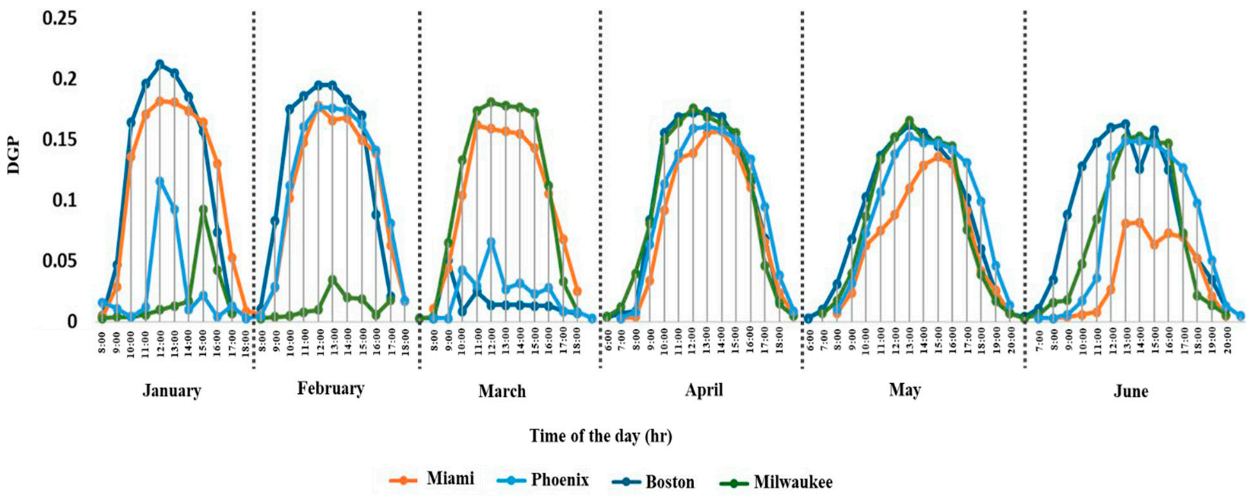

Figure 19. DGP values using horizontal optimum angles on the 21st of the first six months of the year from 8:00 to 18:00.

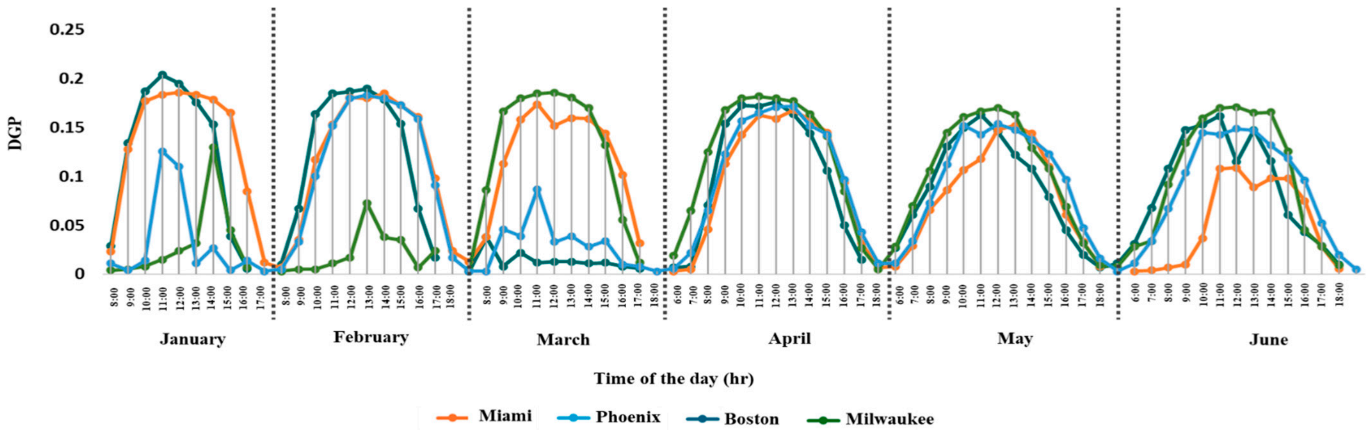

Figure 20. DGP values using vertical optimum angles on the 21st of the first six months of the year from 8:00 to 18:00.

Figures 21–24 illustrate the average annual DGP trends for the horizontal responsive louvers with optimized hourly angles in different facade orientations (south, north, east, and west). The results show that for the south-facing facade with optimized horizontal louvers (Figure 21), Phoenix exhibits the highest average DGP values throughout the year compared to the other cities (0.22 < DGPs < 0.35). In contrast, Milwaukee generally has the lowest DGP values for the south-oriented optimized horizontal louvers (0.13 < DGPs < 0.22). A similar trend is observed for the north-facing facade with optimized horizontal louvers (Figure 22), where Phoenix again demonstrates the highest DGPs, while Boston maintains the lowest values. Examining the east-facing (Figure 23) and west-facing (Figure 24) optimized horizontal louver scenarios, Phoenix continues to have the highest average DGP, while Milwaukee and Boston perform better with lower DGP values, respectively. These findings suggest that the optimized horizontal responsive louver configuration is less effective in managing discomfort glare in hot and dry climates like Phoenix, compared to more temperate and humid climates such as Milwaukee and Boston.

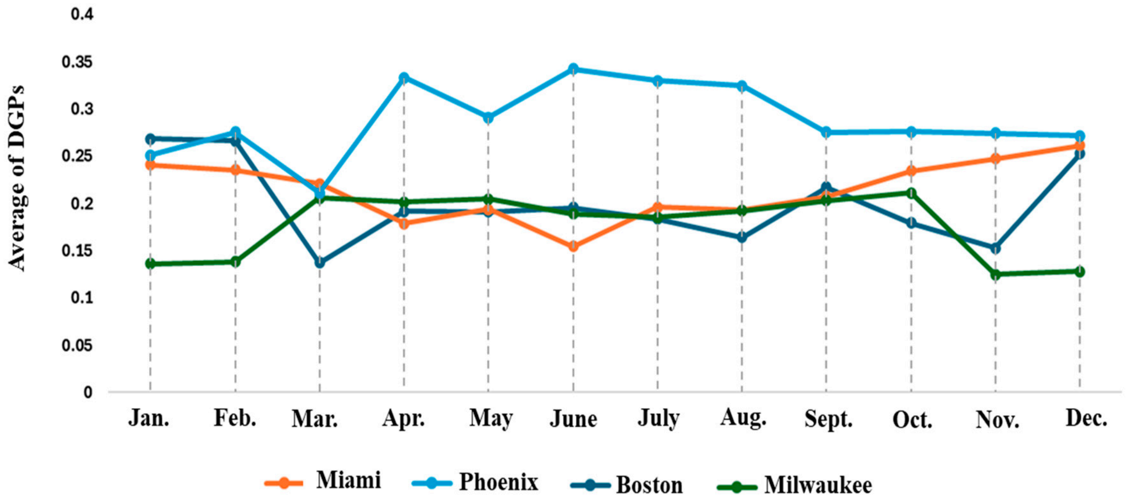

Figure 21. Average annual DGPs of horizontal louvers in the south facade.

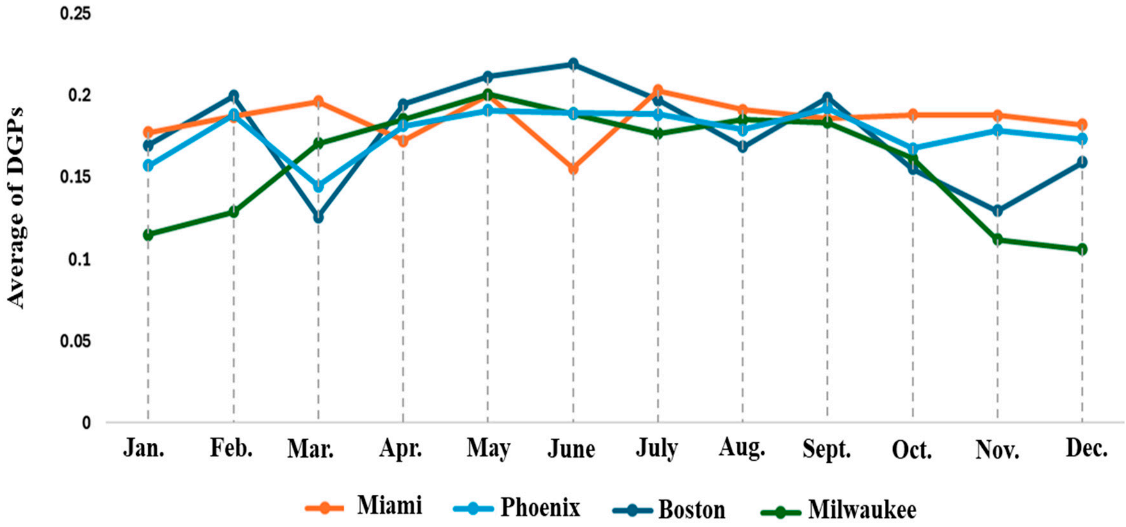

Figure 22. Average annual DGPs of horizontal louvers in the north facade.

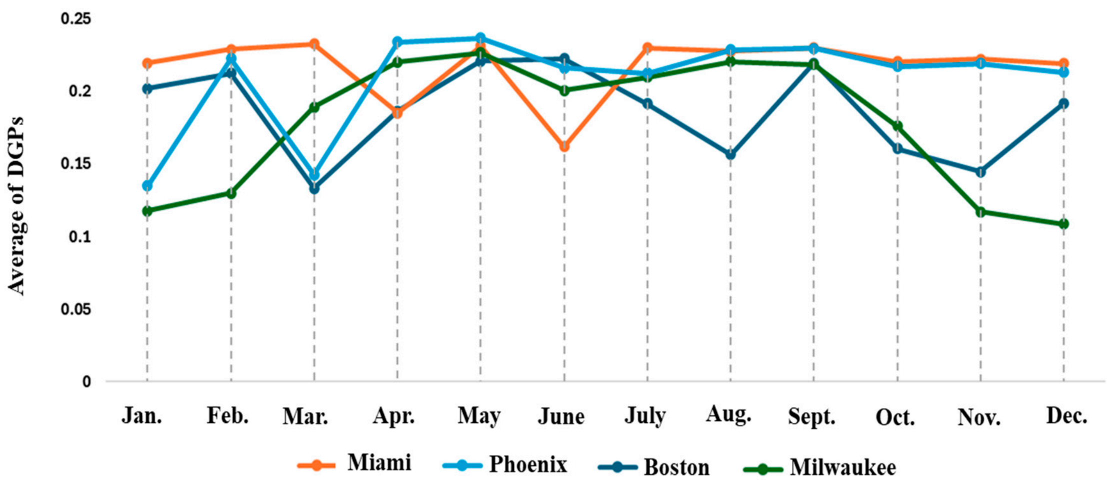

Figure 23. Average annual DGPs of horizontal louvers in the east façade.

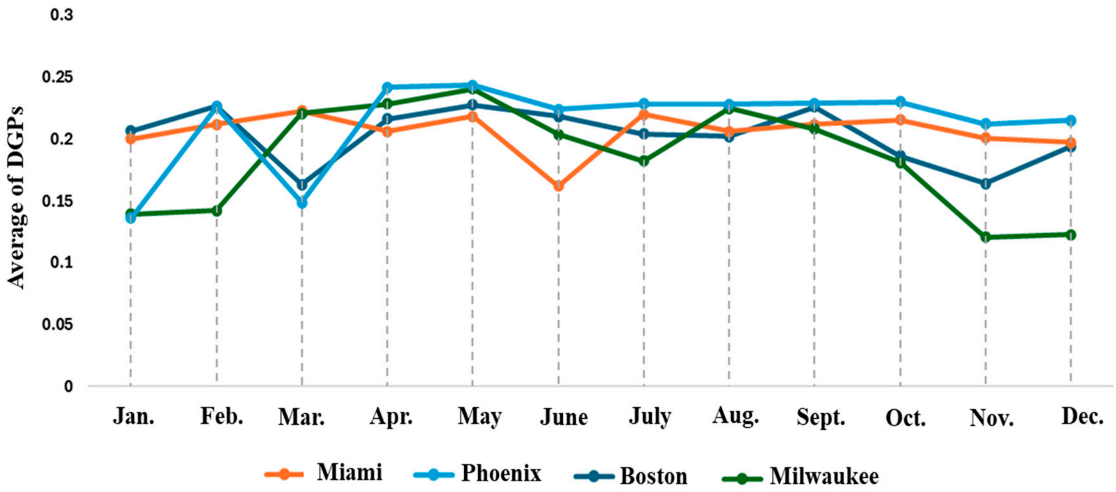

Figure 24. Average annual DGPs of horizontal louvers in the west facade.

Figures 25–28 present the average annual DGP trends for the vertical responsive louvers with optimized hourly angles across the same facade orientations. For the south-facing facade with optimized vertical louvers (Figure 25), Phoenix exhibits the highest DGP values (0.16 < DGPs < 0.29), while Milwaukee demonstrates the lowest (0.12 < DGPs < 0.23). A similar pattern emerges for the north-facing (Figure 26) and east-facing (Figure 27) optimized vertical louver scenarios, with Phoenix having the highest DGP values and Milwaukee the lowest. Interestingly, for the west-facing optimized vertical louvers (Figure 28), Boston shows the highest DGP values, while Milwaukee maintains the lowest. These results indicate that the optimized vertical louver configuration is more effective in managing discomfort glare in Cold–Humid climates like Milwaukee, compared to the Hot–Dry climate of Phoenix or Cool–Humid climate of Boston.

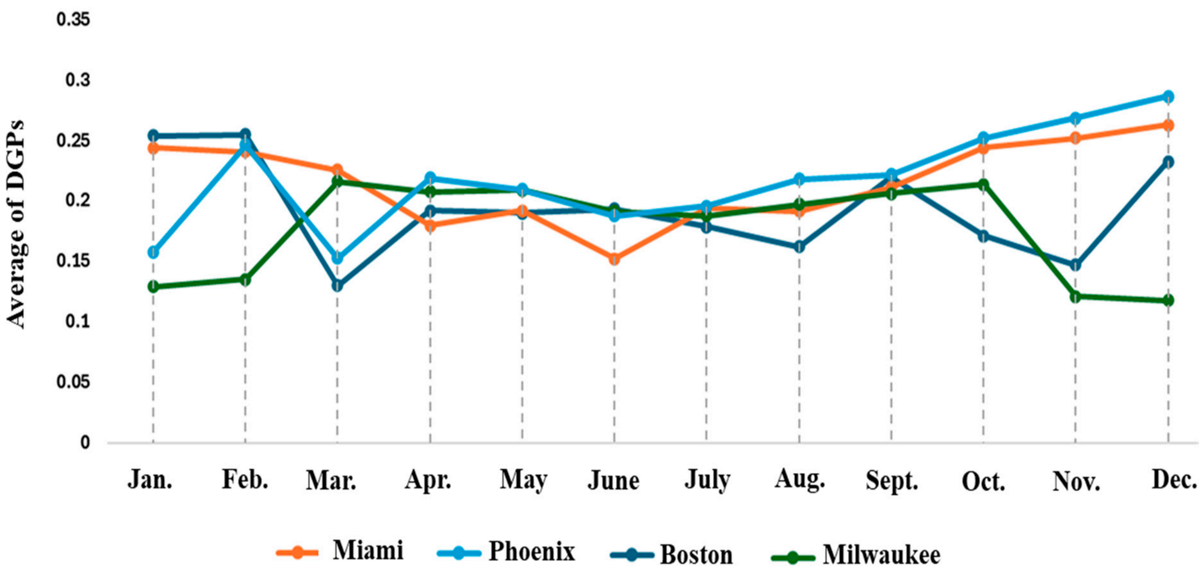

Figure 25. Average annual DGPs of vertical louvers in the south facade.

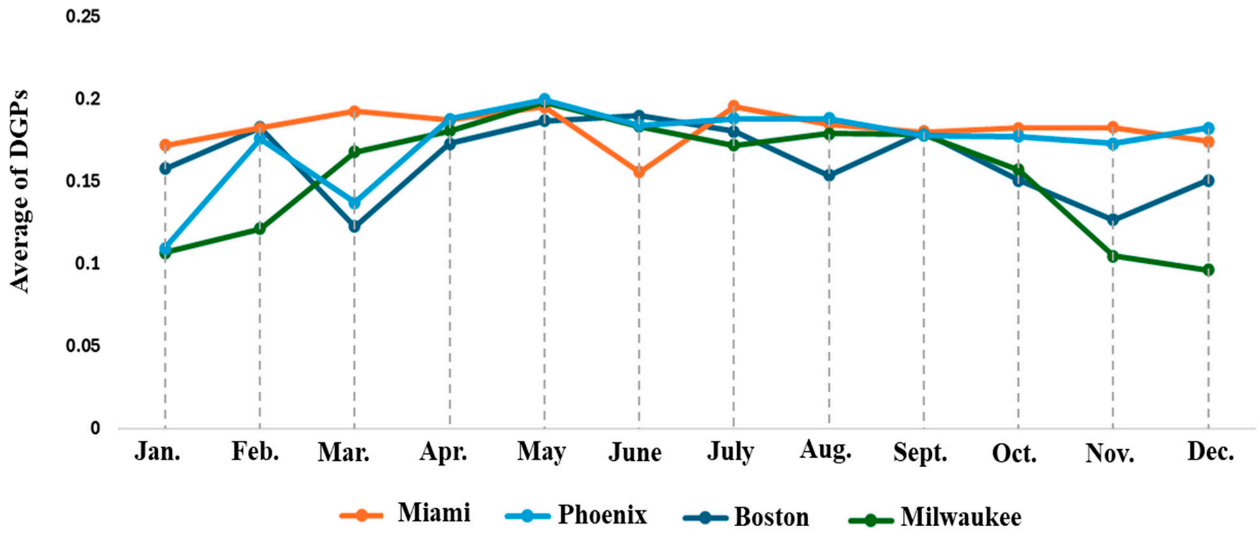

Figure 26. Average annual DGPs of vertical louvers in the north facade.

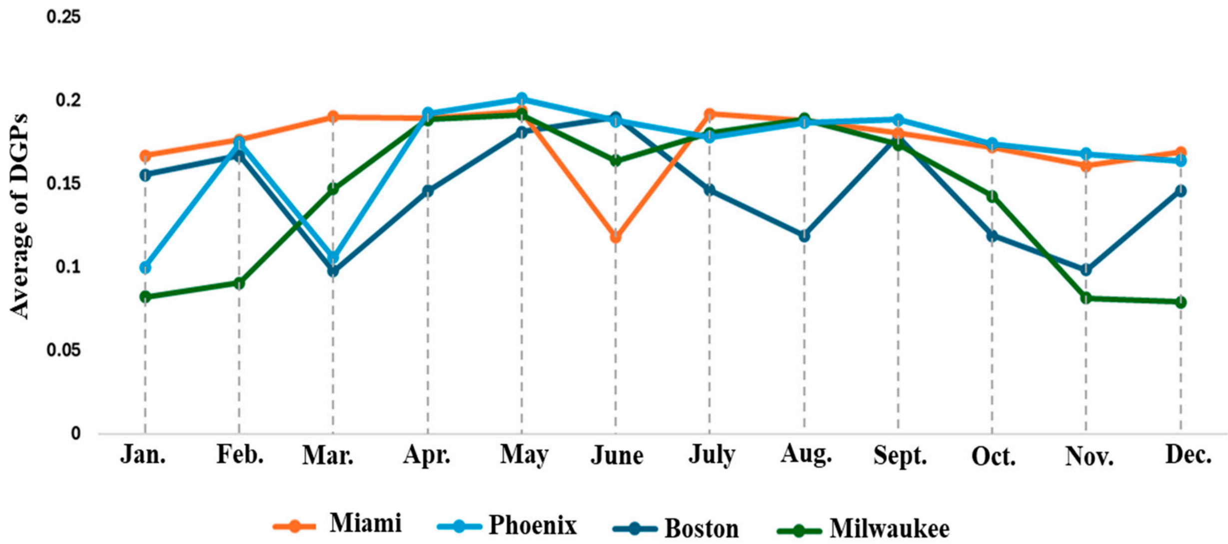

Figure 27. Average annual DGPs of vertical louvers in the east facade.

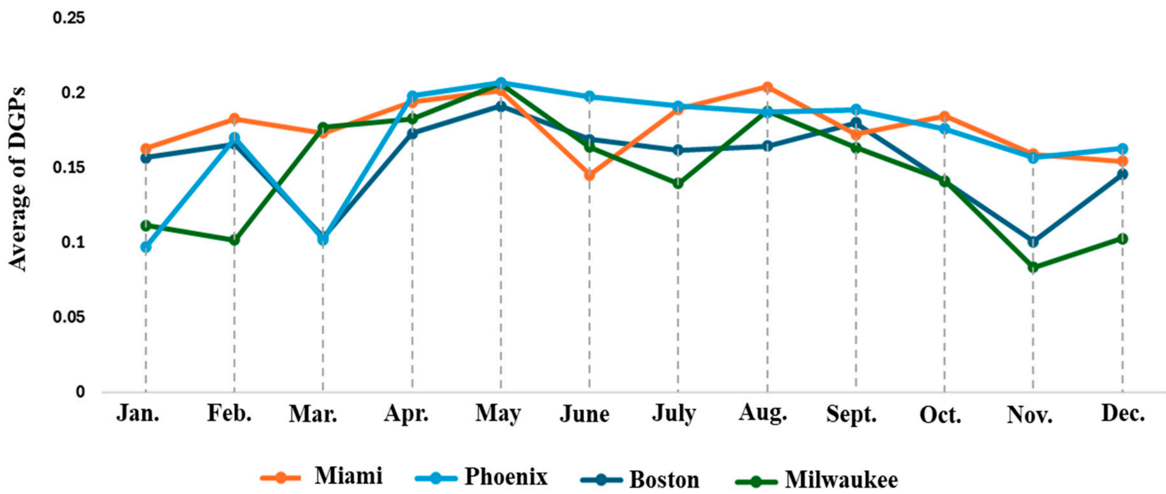

Figure 28. Average annual DGPs of vertical louvers in the west facade.

Considering all the points in the office room, the vertical angles provided more homogenous behavior in April and May for all the cities, while the horizontal results in June show less variation for different cities. In January, the highest value of 0.24 was recorded at noon in Boston when the vertical responsive louvers were adjusted to their optimal angle. Generally, the overall trend seen in the results for vertical configurations is comparable to that of the horizontal configurations.

The analysis of Figures 21–28 indicates that the optimized horizontal responsive louvers generally outperform the optimized vertical louvers in terms of lower average annual DGP values, except for the Milwaukee location, while overall both configurations provided DGP values in the comfort range. This suggests that the optimized horizontal louver configuration is more successful in managing discomfort glare in Cold–Humid and Cool–Humid climates, such as those found in Milwaukee and Boston, compared to Phoenix with Hot–Dry climates. In addition, the optimized vertical louver configuration exhibits better performance in Cold–Humid climates like Milwaukee.

Furthermore, the analysis reveals that the hot and dry climate of Phoenix consistently experiences the highest DGP values across both the optimized horizontal and vertical louver scenarios, signifying that this climate presents the greatest challenge in controlling discomfort glare. Conversely, the cold and humid climate of Milwaukee and the cool and humid climate of Boston generally demonstrate the lowest DGP values, suggesting that these locations are more favorable for effective glare management using the responsive facade strategies explored in this study.

Figures 29 and 30 present the improvement rates of DGPs if optimum hourly angles are applied to horizontal and vertical louvers, respectively. The improvement rate is defined as a quantitative measure that compares the DGP values from scenario ii against scenario i.

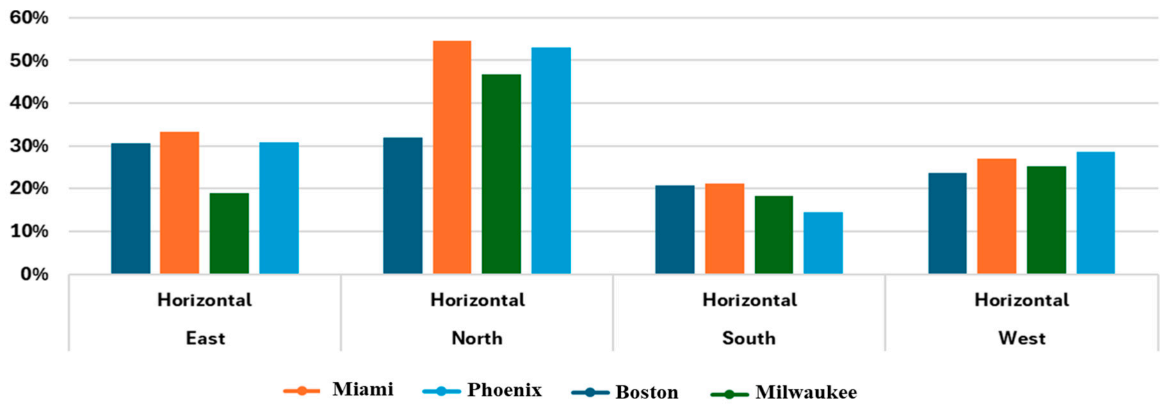

Figure 29. Improvement rate comparisons of different design scenarios when optimum hourly horizontal louvers are used.

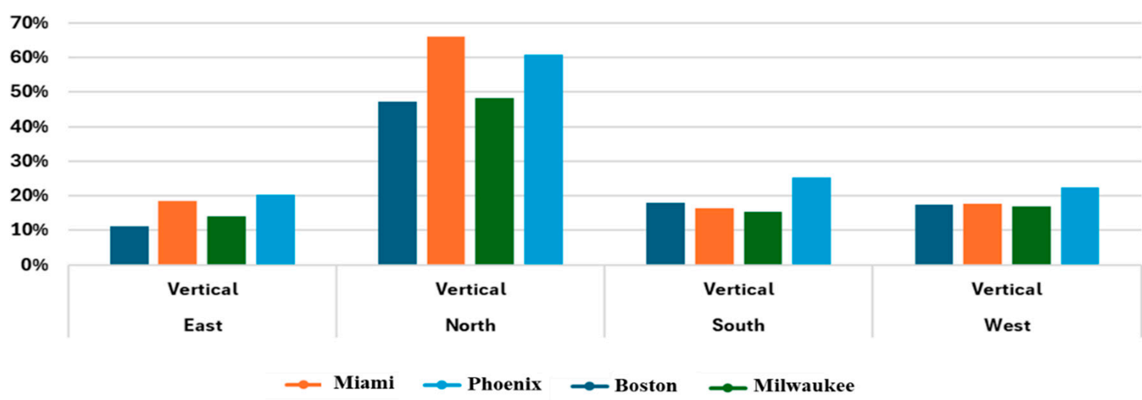

Figure 30. Improvement rate comparisons of different design scenarios when optimum hourly vertical louvers are used.

In the horizontal configuration, Miami demonstrated the best performance in the east, north, and south. Conversely, Phoenix excelled in the west. When utilizing the vertical configuration, Phoenix emerged as the top performer in the east, south, and west, while Miami led in the north.

The improvement rate results indicate that the visual performance of horizontal responsive louvers exceeds that of vertical responsive louvers in the east and south facades across all cities, except for Phoenix, where vertical louvers exhibit better performance. On the other hand, vertical louvers with hourly optimum angles have led to a maximum improvement rate in the north facade in Boston, Miami, Milwaukee, and Phoenix. In the west facade, however, fewer notable differences have occurred in Phoenix and Milwaukee.

A higher improvement rate can improve sustainability indirectly through different channels, such as requiring less artificial light for visual comfort adjustments. This reduction in artificial lighting leads to lower energy consumption, thereby decreasing carbon emissions. Additionally, energy-efficient lighting systems contribute to overall energy savings, enhancing the building's performance. Improved lighting conditions also boost occupants' productivity and well-being, as natural light has been shown to positively impact mood and efficiency. Consequently, these factors collectively contribute to the development of high-performance buildings that are both environmentally friendly and supportive of occupant satisfaction.

In general, by focusing on the simplest configurations of responsive facades, this study simplifies the optimization process, which is often complicated for architects without expertise in computer science. It develops a computational model for minimizing discomfort glare, featuring a replicable step-by-step process with clear input and output data points, which can be utilized by other scholars and architects for both research and practical purposes. The model is versatile and can be repeated and tested for various design scenarios, including more complex responsive facade configurations, different building function types (such as educational, healthcare, and residential), several furniture layouts and furniture materials with various surface reflectivity values, different interior finishes and materials, and diverse climate zones worldwide.

5. Conclusions

This study proposed a data-driven approach to minimize daylight glare probability (DGP) in office environments using responsive facade systems and evaluated its performance across four distinct climate zones in the United States. The findings offer valuable insights for architects, facade designers, and researchers seeking to enhance occupant visual comfort, vision health, and productivity through the design and development of responsive facade strategies.

The results indicate that the optimized horizontal louver configuration generally outperformed the vertical louvers in Hot–Humid, Cold–Humid, and Cool–Humid climates, such as those found in Miami, Milwaukee, and Boston, by achieving lower average annual DGP values. Conversely, the optimized vertical louver design exhibited superior performance in the Cold–Humid climate of Milwaukee, surpassing the horizontal louvers. This suggests that the horizontal louver arrangement is more effective at managing discomfort glare in hot and humid regions, while the vertical louver design is better suited for temperate and humid climates.

Notably, the Hot–Dry climate of Phoenix consistently experienced the highest DGP values across both the optimized horizontal and vertical louver scenarios, underscoring the significant challenge of controlling discomfort glare in this climate type. This observation is aligned with the fact that Phoenix experiences high solar radiation due to its geographical location and clear skies, leading to more direct sunlight and increased glare. Conversely, Cold–Humid climates like Milwaukee generally demonstrated the lowest DGP values, indicating that these locations are more amenable to effective glare management using the responsive facade strategies explored in this study. For Milwaukee, the sun is lower in the sky in winter months, which can lead to more direct sunlight hitting surfaces at angles that produce glare.

Considering building orientations, in the horizontal louver configuration, Miami showed the strongest results in the east, north, and south, while Phoenix stood out in the west. However, with the vertical louver configuration, Phoenix became the leading performer in the east, south, and west, whereas Miami topped the north.

Ultimately, the results showed that responsive louvers with optimum hourly angles could improve discomfort glare in regions with both high and low solar irradiation/low latitude and longitude, which indicates that responsive facades can also be used in cold regions.

One key limitation of the study is the exclusion of the effects of artificial lighting. In real-world scenarios, the presence and characteristics of artificial lighting can significantly impact visual perception and comfort. Incorporating the influence of artificial lighting, such as differences in illumination levels, color temperature, and directionality, would provide a more comprehensive understanding of how visual tasks are carried out in practical settings. Additionally, this study did not account for variations in individual visual capabilities, which can impact the generalizability of the results. Future research should consider a range of visual profiles to better represent the diverse population that would engage in the tasks examined.

The key novelty of this study lies in its comprehensive and systematic approach to evaluating and minimizing discomfort glare in office spaces with responsive facades. Unlike previous research that has typically assessed discomfort glare at a single point or location with a fixed view direction, this work considers multiple influential factors, including the observer's positions and view directions, the hourly active angles of louvers, different facade orientations (north, east, south, west), and varying building locations and climates. By focusing on the active angles of louvers as a design variable, this study develops a computational model to optimize for reduced discomfort glare, which is a novel approach compared to prior work that has mainly concentrated on the general design of responsive facades without explicit glare mitigation. Furthermore, the study utilizes advanced computer-aided design tools to generate, evaluate, and analyze detailed daylight glare probability (DGP) data over the course of a full year, accounting for the hourly adaptation of louver angles in response to changing daylight patterns. This level of holistic simulation and analysis across a range of facade configurations and climate conditions represents a significant advancement over more limited previous investigations on discomfort glare in office environments.

The findings from this study can assist architects, building technologists, and researchers in evaluating the potential for discomfort glare and determining the impact of active design variables in reducing annual glare across different facade configurations, building orientations, and climate zones. By optimizing these variables, buildings can achieve greater energy efficiency and occupant comfort, contributing to overall sustainability. This approach not only minimizes energy consumption and greenhouse gas emissions but also promotes eco-friendly building practices that are essential for sustainable development. The proposed data-driven approach is repeatable and can be utilized and scaled by architects in their design practices to enhance occupant comfort and performance.

Author Contributions: Conceptualization, N.H.M., A.E. and A.G.; Methodology, N.H.M. and A.G.; Validation, A.E. and A.G.; Writing—original draft, N.H.M.; Writing—review & editing, A.E. All authors have read and agreed to the published version of the manuscript.

Funding: The Vice President for Research and Partnership at the University of Oklahoma through the Faculty Investment Program (FIP) funded this project titled "Comprehensive Daylight Optimization for Responsive Facades". In addition, financial support was provided by the University of Oklahoma Libraries' Open Access Fund.

Institutional Review Board Statement: Not applicable.

Informed Consent Statement: Not applicable.

Data Availability Statement: The data presented in this study are available on request from the corresponding author.

Acknowledgments: The Vice President for Research and Partnership at the University of Oklahoma through the Faculty Investment Program (FIP) funded this project titled "Comprehensive Daylight Optimization for Responsive Facades". In addition, financial support was provided by the University of Oklahoma Libraries' Open Access Fund. This project is part of the OU High-Performance Interior Architecture Laboratory (OU-HPIA Lab), which focuses on innovative solutions for sustainable building design.

Conflicts of Interest: The authors declare no conflict of interest.

References

1. Ma, J.H.; Lee, J.K.; Cha, S.H. Effects of lighting CCT and illuminance on visual perception and task performance in immersive virtual environments. *Build. Environ.* **2022**, *209*, 108678. [CrossRef]
2. Kropmana, D.; Appel-Meulenbroeka, R.; Bergefurta, L.; LeBlanc, P. The business case for a healthy office; a holistic overview of relations between office workspace design and mental health. *Ergonomics* **2023**, *66*, 658–675. [CrossRef] [PubMed]
3. Carlucci, F.; Causone, F.; De Rosa, F.; Pagliano, L. A review of indices for assessing visual comfort with a view to their use in optimization processes to support building integrated design. *Renew. Sustain. Energy Rev.* **2015**, *47*, 1016–1033. [CrossRef]
4. Hosseini, S.M.; Mohammadi, M.; Rosemann, A.; Schröder, T. Quantitative Investigation Through Climate-based Daylight Metrics of Visual Comfort Due to Colorful Glass and Orosi Windows in Iranian Architecture. *J. Daylighting* **2018**, *5*, 21–33. [CrossRef]
5. Boyce, P.R. *Human Factors in Lighting*, 3rd ed.; Taylor & Fancis Group: Abingdon, UK, 2014.
6. [CIE] Commission Internationale on Illumination (Commission Internationale de L'éclairage). *CIE e-ILV Term 17-492 Glare*; CIE: Vienna, Austria, 2019; Available online: https://cie.co.at/e-ilv (accessed on 16 October 2019).
7. Fotios, S.; Kent, M. Measuring Discomfort from Glare: Recommendations for Good Practice. *J. Illum. Eng. Soc. (Leukos)* **2020**, *17*, 338–358. [CrossRef]
8. Osterhaus, W.K.E. Discomfort glare assessment and prevention for daylight applications in office environments. *Sol. Energy* **2005**, *79*, 140–158. [CrossRef]
9. Haapakangas, A.; Keränen, J.; Nyman, M.; Hongisto, V. Lighting improvement and subjective working conditions in an industrial workplace. *Light Eng.* **2012**, *20*, 86–96.
10. Chen, R.; Meng-Chun, T.; Yaw-Shyan, T. Effect of Color Temperature and Illuminance on Psychology, Physiology, and Productivity: An Experimental Study. *Energies* **2022**, *15*, 4477. [CrossRef]
11. Duijnhoven, J.; Aarts, M.P.J.; Aries, M.B.C.; Rosemann, A.L.P.; Kort, H.S.M. Systematic review on the interaction between office light conditions and occupational health: Elucidating gaps and methodological issues. *Indoor Built Environ.* **2019**, *28*, 152–174. [CrossRef]
12. Kim, J.; Dear, R. Nonlinear relationships between individual IEQ factors and overall workspace satisfaction. *Build. Environ.* **2012**, *49*, 33–40. [CrossRef]
13. Chellappa, S.L.; Steiner, R.; Blattner, P.; Oelhafen, P.; Götz, T.; Cajochen, C. Non-visual effects of light on melatonin, alertness and cognitive performance: Can blue-enriched light keep us alert? *PLoS ONE* **2011**, *6*, e16429. [CrossRef] [PubMed]
14. Reinhart, C.F. *Daylighting Handbook II. Daylight Simulations. Dynamic Facades*; Building Technology Press: Cambridge, MA, USA, 2018.
15. Reinhart, C.F.; Mardaljevic, J.; Rogers, Z. Dynamic daylight performance metrics for sustainable building design. *Leukos* **2006**, *3*, 7–31. [CrossRef]
16. Giovannini, L.; Favoino, F.; Lo Verso, V.R.M.; Pellegrino, A.; Serra, V. A Simplified Approach for the Annual and Spatial Evaluation of the Comfort Classes of Daylight Glare Using Vertical Illuminances. *Buildings* **2018**, *8*, 171. [CrossRef]
17. Chiaraviglio, L. Assessment of Discomfort Glare in Daylit Rooms with Shading Devices: Results from a Field Study and Comparison with Software Simulation. Ph.D. Thesis, Politecnico di Torino, Turin, Italy, 2009.
18. Suk, J.; Schiler, M. Investigation of Evalglare software, daylight glare probability and high dynamic range imaging for daylight glare analysis. *Light. Res. Technol.* **2013**, *45*, 450–463. [CrossRef]

19. Andersen, M.; Gochenour, S.; Lockley, S. Modelling 'non-visual' effects of daylighting in a residential environment. *Build. Environ.* **2013**, *70*, 138–149. [CrossRef]
20. Chaloeytoy, K.; Ichinose, M.; Chien, S.-C. Determination of the Simplified Daylight Glare Probability (DGPs) Criteria for Daylit Office Spaces in Thailand. *Buildings* **2020**, *10*, 180. [CrossRef]
21. Suk, J.; Schiler, M.; Kensek, K. Development of new daylight glare analysis methodology using absolute glare factor and relative glare factor. *Energy Build.* **2013**, *64*, 113–122. [CrossRef]
22. Pierson, C.; Wienold, J.; Bodart, M. Discomfort glare perception in daylighting: Influencing factor. *Energy Procedia* **2017**, *122*, 331–336. [CrossRef]
23. Tabadkani, A.; Banihashemi, S.; Hosseini, M.R. Daylighting and visual comfort of oriental sun responsive skins: A parametric analysis. *Build. Simul.* **2018**, *11*, 663–676. [CrossRef]
24. O'Brien, W.; Kapsis, K.; Athienitis, A.K. Manually-operated window shade patterns in office buildings: A critical review. *Build. Environ.* **2013**, *60*, 319–338. [CrossRef]
25. Grobman, Y.J.; Austern, G.; Hatiel, R.; Capeluto, I.G. Evaluating the Influence of Varied External Shading Elements on Internal Daylight Illuminances. *Buildings* **2020**, *10*, 22. [CrossRef]
26. Matin, N.H.; Eydgahi, A. Technologies used in responsive facade systems: A comparative study. *Intell. Build. Int.* **2022**, *14*, 54–73. [CrossRef]
27. Heidari Matin, N.; Eydgahi, A.; Shyu, S.; Matin, P. Evaluating Visual Comfort Metrics of Responsive Facade Systems as Educational Activities. In Proceedings of the Annual Conference of American Society for Engineering, Salt Lake City, UT, USA, 24–27 June 2018.
28. Loonen, R.; Trčka, M.; Cóstola, D.; Hensen, J.L.M. Climate Adaptive Building Shells: State-of-the-art and Future Challenges. *Renew. Sustain. Energy Rev.* **2013**, *25*, 483–493. [CrossRef]
29. Shan, R. Climate Responsive Façade Optimization Strategy. Ph.D. Thesis, University of Michigan, Ann Arbor, MI, USA, 2016. Available online: https://deepblue.lib.umich.edu/handle/2027.42/133475 (accessed on 14 September 2019).
30. Shan, R.; Junghans, L. "Adaptive Radiation" Optimization for Climate Adaptive Building Facade Design Strategy. *Build. Simul.* **2017**, *11*, 269–279. [CrossRef]
31. Heidari Matin, N.; Eydgahi, A. A data-driven optimized daylight pattern for responsive facades design. *Intell. Build. Int.* **2021**, *14*, 363–374. [CrossRef]
32. Tabadkani, A.; Roetzel, A.; Li, H.X.; Tsangrassoulis, A. A review of automatic control strategies based on simulations for adaptive facades. *Build. Environ.* **2020**, *175*, 106801. [CrossRef]
33. Loonen, R.; Rico-Martinez, J.; Favoino, F.; Marcin, B. Design for façade adaptability—Towards a unified and systematic characterization. In Proceedings of the Conference Proceedings of the 10th Energy Forum, Bern, Switzerland, 3–4 November 2015.
34. Hosseini, S.M.; Mohammadi, M.; Guerra-Santin, O. Interactive kinetic façade: Improving visual comfort based on dynamic daylight and occupant's positions by 2D and 3D shape changes. *Build. Environ.* **2019**, *165*, 106396. [CrossRef]
35. Wagdy, A.; Fathy, F.; Altomonte, S. Evaluating the daylighting performance of dynamic façades by using new annual climate-based metrics. In Proceedings of the 32nd International Conference on Passive and Low Energy Architecture, Los Angeles, CA, USA, 11–13 July 2016; Volume 2, pp. 941–947.
36. Besbas, S.; Nocera, F.; Zemmouri, N.; Khadraoui, M.A.; Besbas, A. Parametric-Based Multi-Objective Optimization Workflow: Day-light and Energy Performance Study of Hospital Building in Algeria. *Sustainability* **2022**, *14*, 12652. [CrossRef]
37. Valitabar, M.; GhaffarianHoseini, A.; Ghaffarian Hoseini, A.; Attia, S. Advanced control strategy to maximize view and control discomforting glare: A complex adaptive façade. *Archit. Eng. Des. Manag.* **2022**, *18*, 829–849. [CrossRef]
38. Tabadkani, A.; Shoubi, M.V.; Soflaei, F.; Banihashemi, S. Integrated parametric design of adaptive facades for user's visual comfort. *Autom. Constr.* **2019**, *106*, 102857. [CrossRef]
39. Hosseini, S.M.; Fadli, F.; Mohammadi, M. Biomimetic Kinetic Shading Facade Inspired by Tree Morphology for Improving Occupant's Daylight Performance. *J. Daylighting* **2021**, *8*, 65–82. [CrossRef]
40. Toodekharman, H.; Abravesh, M.; Heidari, S. Visual Comfort Assessment of Hospital Patient Rooms with Climate Responsive Facades. *J. Daylighting* **2023**, *10*, 17–30. [CrossRef]
41. Mehrvarz, F.; Bemanian, M.; Nasr, T.; Mansoori, R.; ALKazee, M.; Khudhayer, W.; Mahdavinejad, M. Designerly Approach to Design Responsive Facade for Occupant Visual Comfort in Different Latitudes. *J. Daylighting* **2024**, *11*, 149–164. [CrossRef]
42. Sommese, F.; Hosseini, S.; Badarnah, L.; Capozzi, F.; Giordano, S.; Ambrogi, V.; Ausiello, G. Light-responsive kinetic façade system inspired by the Gazania flower: A biomimetic approach in parametric design for daylighting. *Build. Environ.* **2024**, *247*, 111052. [CrossRef]
43. Yi, H.; Kim, M.-J.; Kim, Y.; Kim, S.-S.; Lee, K.-I. Rapid Simulation of Optimally Responsive Façade during Schematic Design Phases: Use of a New Hybrid Metaheuristic Algorithm. *Sustainability* **2019**, *11*, 2681. [CrossRef]
44. Kızılörenli, E.; Maden, F. Modular responsive facade proposals based on semi-regular and demi-regular tessellation: Daylighting and visual comfort. *Front. Archit. Res.* **2023**, *12*, 601–612. [CrossRef]

45. Özdemir, H.; Çakmak, B.Y. Evaluation of Daylight and Glare Quality of Office Spaces with Flat and Dynamic Shading System Facades in Hot Arid Climate. *J. Daylighting* **2022**, *9*, 197–208. [CrossRef]
46. Matin, N.H.; Eydgahi, A.; Gharipour, A. Computer-Aided Design Application in Determining Minimum Discomfort Glare. In Proceedings of the 2023 IEEE 6th International Conference on Knowledge Innovation and Invention (ICKII), Sapporo, Japan, 11–13 August 2023; pp. 303–308. [CrossRef]
47. Lacanna, G.; Wagenaar, C.; Avermaete, T.; Swami, V. Evaluating the Psychosocial Impact of Indoor Public Spaces in Complex Healthcare Settings. *Health Environ. Res. Des. J.* **2019**, *12*, 11–30. [CrossRef] [PubMed]
48. Reinhart, C.F. Lightswitch-2002: A model for manual and automated control of electric lighting and blinds. *Sol. Energy* **2004**, *77*, 15–28. [CrossRef]
49. Wienold, J.; Christoffersen, J. Evaluation methods and development of a new glare prediction model for daylight environments with the use of CCD cameras. *Energy Build.* **2006**, *38*, 743–757. [CrossRef]
50. Hafiz, D. Daylighting, space, and architecture: A literature review. *Enq. ARRC J. Archit. Res.* **2015**, *12*, 2329–9339. [CrossRef]
51. Kurnia, K.; Azizah, D.; Mangkuto, R.; Atmodipoero, R. Visual comfort assessment using high dynamic range images under daylight condition in the main library building of Institut Teknologi Bandung. *Procedia Eng.* **2017**, *170*, 234–239. [CrossRef]
52. Ng, E.Y.-Y.; Poh, L.K.; Wei, W.; Nagakura, T. Advanced lighting simulation in architectural design in the tropics. *Autom. Constr.* **2001**, *10*, 365–379. [CrossRef]
53. Yoon, Y.; Moon, J.W.; Kim, S. Development of annual daylight simulation algorithms for prediction of indoor daylight illuminance. *Energy Build.* **2016**, *118*, 1–17. [CrossRef]
54. Nezamdoost, A.; Van Den, W.; Kevin, G. Revisiting the Daylit Area: Examining Daylighting Performance Using Subjective Human Evaluations and Simulated Compliance with the LEED Version 4 Daylight Credit. *J. Illum. Eng. Soc.* **2017**, *13*, 107–123. [CrossRef]
55. Stringham, J.M.; Garcia, P.V.; Smith, P.A.; McLin, L.N.; Foutch, B.K. Macular pigment and visual performance in glare: Benefits for photostress recovery, disability glare, and visual discomfort. *Investig. Ophthalmol. Vis. Sci.* **2011**, *52*, 7406–7415. [CrossRef] [PubMed]
56. Gharipour, A.; Liew, A.W.-C. An integration strategy based on fuzzy clustering and level set method for cell image segmentation. In Proceedings of the 2013 IEEE International Conference on Signal, Communication and Computing, Kunming, China, 5–8 August 2013.
57. Gharipour, A.; Liew, A.W.-C. Level set-based segmentation of cell nucleus in fluorescence microscopy images using correntropy-based K-means clustering. In Proceedings of the 2015 International Conference on Digital Image Computing: Techniques and Applications (DICTA), Adelaide, Australia, 23–25 November 2015.
58. Pacific Northwest National Laboratory (NPPL). *U.S. Department of Energy. Annual Site Environmental Report*; The U.S. Department of Energy: Oak Ridge, TN, USA, 2015; p. 155.
59. Verma, R.; Dhanda, N.; Nagar, V. Enhancing Security with In-Depth Analysis of Brute-Force Attack on Secure Hashing Algorithms. In Proceedings of the Trends in Electronics and Health Informatics, Kanpur, India, 16–17 December 2021; Springer: Singapore, 2022; p. 376. [CrossRef]
60. Trakhtenbrot, B. A Survey of Russian Approaches to Perebor (Brute-Force Searches) Algorithms. *IEEE Ann. Hist. Comput.* **1984**, *6*, 384–400. [CrossRef]
61. Liu, C.; Zhang, F.; Zhang, H.; Shi, Z.; Zhu, H. Optimization of assembly sequence of building components based on simulated annealing genetic algorithm. *Alex. Eng. J.* **2023**, *62*, 257–268. [CrossRef]
62. Allam, A.S.; Bassioni, H.; Ayoub, M.; Kamel, W. Investigating the performance of genetic algorithm and particle swarm for optimizing daylighting and energy performance of offices in Alexandria, Egypt. *Smart Sustain. Built Environ.* **2023**, *12*, 682–700. [CrossRef]
63. Rezakhani, M.; Sung-Ah, K. Genetic Algorithm-Driven Optimization of Pattern for Parametric Facade Design Based on Support Position Data to Increase Visual Quality. *Buildings* **2024**, *14*, 1086. [CrossRef]
64. Peña-García, A. Sustainability as the Key Framework of a Total Lighting. *Sustainability* **2018**, *10*, 4412. [CrossRef]